

Modelling the long-term impacts of artificial warming on the Martian water cycle and surface ice distribution.

Ashwin S. Braude,¹

Edwin S. Kite,^{1,2}

Mark I. Richardson,³

Alexandre Kling,¹

and Michael A. Mischna,⁴

¹Astera Institute, Emeryville, CA, USA

²Department of the Geophysical Sciences, University of Chicago, Chicago, IL, USA

³Aeolis Research, Chandler, AZ, USA.

⁴Jet Propulsion Laboratory, California Institute of Technology, Pasadena, CA, USA

arXiv:2603.01539v1 [astro-ph.EP] 2 Mar 2026

Abstract

Recent papers by Ansari et al. (2024, *Science Advances* 10, eadn4650) and Richardson et al. (2025, arXiv eprint 2504.01455) have suggested that global warming of the Martian surface (‘terraforming’) by 35 K to sustain local habitats above the melting point of water could be achieved through the injection of engineered aerosols into the Martian atmosphere. Using the MarsWRF 3D Global Climate Model, we investigate how artificial warming of Mars through engineered aerosol release would affect the planetary water cycle and the distribution of the major surface ice reservoirs. Within our model framework, every 20 K of global warming induces a tenfold increase in atmospheric water vapour content due to sublimation of H₂O ice from the North Polar Cap. This increases the potency of cloud radiative feedbacks which induces nighttime warming (~5-10 K) at low latitudes, but daytime cooling (up to 40 K) in the winter midlatitudes. Water is transferred from the edge of the North Polar Cap to the South Polar Cap and there is minor destabilisation of shallow northern midlatitude subsurface ice. As a result, seasonal sublimation of H₂O ice from the South Pole has an increased impact on the global water cycle. These changes persist on Mars at least decades after loading of the atmosphere with engineered aerosols ceases. Our model is limited by the gaps in our knowledge of present-day Martian weather and climate, and of the microphysics and radiative properties of candidate warming agents. Much more data is therefore needed before warming Mars could become feasible.

1 Introduction

Although the Martian surface today is too cold and dry to sustain liquid water, overwhelming evidence shows that it was once warmer and wetter (e.g. Craddock & Howard, 2002; Hynek et al., 2010; Kite & Conway, 2024; Mondro et al., 2025), and may still be sufficiently warm in the subsurface for groundwater (Grimm et al., 2017). Mars will naturally rewarm as the Sun brightens, but this will take billions of years and, if the water escapes into space, may result in a Mars that is even drier than it is today (Jakosky, 2024). Previous studies (McKay et al., 1991; Zubrin & McKay, 1997; DeBenedictis et al., 2025) have therefore assessed the feasibility of restoring a warm and wet Mars artificially using existing readily-available resources on the planet. Making Mars’ environment more suitable for life faces many challenges including extreme cold, and a 6 mbar atmosphere that lacks oxygen and that fails to block damaging ultraviolet radiation. This is because much of Mars’ ancient atmosphere was lost to space (Jakosky et al., 2018), while known reserves of CO₂ ice on Mars could only double the present-day atmospheric pressure (Jakosky

& Edwards, 2018; Forget et al., 2024), which is not sufficient to induce runaway warming (Sagan, 1973; McKay et al., 1991).

Studies in the early 2000s (Gerstell et al., 2001; Marinova et al., 2005; Dicaire et al., 2013) focussed on warming Mars by >30 K using a C_3F_8 -dominated mix of super-greenhouse gases, but this would require $O(10^{14})$ kg of fluorine - a scarce quantity in Mars soil (Forni et al., 2015; Rampe et al., 2018) - to produce. More recently, a range of alternative methods have been proposed to warm Mars, including through the solid-state greenhouse effect (Wordsworth et al., 2019; Wordsworth & Cockell, 2024) and with orbiting reflectors (Handmer, 2024). In this paper, we focus on the method proposed by Ansari et al. (2024) and Richardson et al. (2025) respectively (hereon referred to as “A24” and “R25”), that involves releasing artificial ‘engineered’ aerosols into the Martian atmosphere optimised to induce a powerful greenhouse effect by allowing sunlight to reach the surface, while redirecting upwelling thermal infrared radiation back to the surface. A24 and R25 suggest that these aerosols could warm Mars by >30 K in ~ 2 Mars years at current atmospheric pressure, with feedstock obtained either from the soil in the case of metal particles (Williams et al., 1979), or from the electrolysis of Mars’ CO_2 atmosphere (Hoffman et al., 2022). This would be sufficient to sustain liquid water in the near-surface, which is one of several necessary prerequisites for microbes to thrive in Martian soil (DeBenedictis et al., 2025). On the other hand, it may not necessarily be desirable to warm Mars even if it scientifically feasible to do so. Ethical arguments (e.g. Marshall, 1993; Haqq-Misra, 2012; Schwartz, 2013; Stoner, 2021; Forget et al., 2024) against artificial warming include Mars’ astrobiological and broader scientific value in its current virtually unmodified state. Creation of local habitats will therefore precede and take priority over global terraforming. Furthermore, secondary climate feedbacks on Mars could result in unforeseen consequences on the Martian climate system that could counter any efforts to create habitable environments on Mars, or indeed even make Mars less habitable. This therefore motivates us to further study the effect of these climate feedbacks on an artificially warmed Mars, and to ensure that attempts to modify the Martian climate take into account the possibility of an ‘off-switch’ (Kite & Wordsworth, 2025), where the planet can be restored to its pre-terraformed state if desired.

Previous studies on this subject neglected a critical component of the Martian climate system which could potentially undermine efforts to increase its habitability: the response of the water cycle to artificial warming. Mars has $>5 \times 10^6$ km³ water ice (Carr & Head, 2015; Jakosky & Hallis, 2024), stored in ice caps over both poles, and in shallow-buried midlatitude ice deposits (reviewed in Morgan et al., 2025) that may have formed during periods of high obliquity within

the last million years (Leighton & Murray, 1966; Schörghofer & Forget, 2012; Aharonson et al., 2026). Mars' seasonal water cycle is presently dominated by the summer sublimation of the North Polar Cap. Each Mars year, $\sim 1 \text{ km}^3$ of H_2O sublimates from the North Polar ice Cap, which partly condenses out of the atmosphere as clouds, and is deposited seasonally onto the surface as frost that then resublimates later in the year (see Montmessin et al. (2017) for a review). By contrast, dust lag deposits and a permanent layer of CO_2 ice prevent water ice in the South Polar Cap from sublimating, which therefore only plays a minor role in the Martian seasonal water cycle. Simulations of recent Mars at high obliquity (Haberle et al., 2003; Levrard et al., 2004; Mischna et al., 2003; Forget et al., 2006; Madeleine et al., 2009, 2014; Naar, 2023) show that warming the North Polar Cap would cause a) an increased concentration of water vapour in the atmosphere, and correspondingly more water-vapour greenhouse warming, b) more cloud formation, which can either heat or cool the surface (Madeleine et al., 2012, 2014; Kite et al., 2021) and c) more seasonal surface frost (Bapst et al., 2015; Lange et al., 2024) at low latitudes, which would reflect more sunlight to space. Changes to Mars' water cycle through artificial warming could therefore warm or cool Mars through complicated cloud radiative feedbacks (Haberle, 2013; Madeleine et al., 2014; Kite et al., 2021). In addition, simulations of the water cycle on early Mars show that warming can destabilise water ice reservoirs in the midlatitudes, which are valuable as a future source of propellant and drinking water, as well as being a scientific record of climatic change in the last 0.1%-1% of Mars' history (Bramson et al., 2021; Becerra et al., 2021). Studies of the early Martian climate suggest that a warmer Mars could result in an 'icy highlands' scenario (Wordsworth et al., 2013, 2015), where surface ice shifts to high elevations. Here, the low atmospheric pressure would render the ice especially resistant to melting and sublimation, thereby making the return of the ice to its original location difficult, and hindering its use for human exploration. Moreover, water ice is subject to negative feedbacks that make it resistant to warming. Firstly, ice can reflect more sunlight than bare ground, which helps to keep it cool and stabilise it against sublimation ("ice-albedo feedback"). Conversely, faster sublimation in a warmed climate would increase evaporitic cooling of warm ice, which can prevent surface melting (Ingersoll, 1970; Schörghofer, 2020; Khuller & Clow, 2024). Ice that has shifted in a warmed climate might therefore take decades or longer to revert to its original location if a decision was made to stop warming. Understanding all of these effects on the water cycle induced by artificial warming is therefore of basic scientific interest.

Here, we use a 3-D Global Climate Model (GCM) to assess the water cycle response to engineered Mars warming, including temperature feedbacks and possible "tipping points" in wa-

ter ice distribution. In particular, we wish to address a) the effect of radiative cloud feedbacks on surface temperatures, b) changes in the distribution of surface and near-surface ice, and c) the reversibility of any of these changes on decade-long timescales. In section 2 we describe our model and idealised warming agent. In section 3 we present our results on the effect of aerosol release on surface temperatures and atmospheric water concentration. In section 4 we then present the results of our model when engineered aerosol release is ceased, and how this would affect the planet's surface ice reservoirs. Section 5 discusses data and model limitations that prevent the resolution of open questions about Mars warming, and final conclusions are presented in Section 6.

2 Model

To model Mars' climate, we use the Mars version of the Planet Weather and Research Forecasting (MarsWRF) 3-D GCM (Michalakes et al., 2004; Skamarock et al., 2005; Richardson et al., 2007; Toigo et al., 2012). We run MarsWRF at 60×36 spatial resolution (longitude \times latitude), with 52 vertical layers parametrised in modified-sigma coordinates from the surface to a top of atmosphere located at ~ 120 km altitude to allow for an increase in the height of the Hadley Cell circulation induced by artificial warming. We do not model a thermosphere for the topmost layer of the atmosphere (spanning altitudes from 80 to 120 km) and instead assume the atmosphere to be well-mixed over all altitudes. We use smoothed Martian topography (with a 5-point nearest neighbour smoother at the resolution of the model) to minimise dynamical instabilities in the model caused by sharp topographic features such as Olympus Mons. We use a two-stream radiative transfer scheme with gas absorption modelled according to the correlated-k approximation (Mischna et al., 2012). Outgoing longwave radiation is binned into seven individual spectral bands from 4.5 to 1000 microns, while incoming solar radiation is binned into seven spectral bands from 0.25 to 4.5 microns. Our model approximations result in net energy leakage into space of $2\text{-}3 \text{ W m}^{-2}$ from the top of the atmosphere averaged over the Martian year. In these simulations, we neglect both dust microphysics and dust-water ice coupling. Instead, we prescribe seasonal changes in background dust optical depth according to the MY 36 non-Global Dust Storm scenario of Montabone et al. (2015, 2020). Water ice cloud particles are assumed to all be of equal radius, and form when the water vapour content achieves 100% saturation, with optical constants described in Iwabuchi and Yang (2011). In our model, this size is fixed at $5 \mu\text{m}$ effective radius, in line with observed values in the Aphelion Cloud Belt (Atwood et al., 2024). Sublimation and deposition of surface water ice is modelled as described in Lee et al. (2018), with the albedo and

emissivity of the surface only updated to the prescribed values for water ice if the amount of water ice on the surface is greater than 5 g m^{-2} .

We cap the surface temperature at the South Pole poleward of 85° S to be below the frost point of CO_2 in order to maintain a residual South Polar Cap for modern Mars conditions. We assume values of surface albedo and emissivity of 0.78 and 0.48 respectively for north polar CO_2 ice, and 0.43 and 0.747 respectively for south polar CO_2 ice, which were derived empirically through model tuning to atmospheric pressure variations observed by the Viking lander (Guo et al., 2009). The albedo of south polar CO_2 ice is underestimated in our model relative to observations (e.g. Colaprete et al., 2005; Schmidt et al., 2009; Pommerol et al., 2011; Gary-Bicas et al., 2020). However, the behaviour of the residual South Polar Cap is also not fully understood and exhibits high interannual variability (James et al., 2001, 2007). As with most other models (e.g. Buhler et al., 2020), a high CO_2 albedo in our model in line with observed values results in an overestimate of the amount of annual CO_2 ice deposition on and around the residual south polar cap. This, in turn, causes water ice to be too resistant to sublimation in summer, resulting in a high net annual accumulation of ice over the South Pole that is not in line with observations. The default properties of the South Polar CO_2 ice were therefore chosen to compromise between their observed values and how they affect the water and CO_2 cycle in our model. Nonetheless, in order to ascertain the sensitivity of the water cycle to the properties of the South Polar Cap under both control and warmed scenarios, we also ran an additional set of simulations in which temperatures at the South Pole were allowed to exceed the frost point of CO_2 and where emissivity of the South Polar Cap was decreased to 0.6. We ignore the effect of artificial heating not only on the change in albedo of the South Polar cap, but also on the destabilisation of buried CO_2 ice deposits there, which could potentially double Mars' atmospheric pressure (Buhler et al., 2020). In practice, this release would be slowed by the latent heat of sublimation of CO_2 ice, with the full sublimation of the known CO_2 likely taking >100 years.

To initialise the model, we add a perennial North Polar ice cap down to 80° N for latitudes between -180° and 115° E , and down to 85° N at other longitudes (with an additional detached section of perennial water ice between latitudes of longitudes of 120° - 180° E) to represent the approximate size of the observed perennial cap. We parametrise this cap as a quasi-infinite reservoir of water ice with an assumed fixed albedo as a variable parameter - by default we use 0.4, but we also perform model runs with 0.35 and 0.45 (Wilson et al., 2007; Navarro et al., 2014). We assume a global mean surface pressure of 610 Pa and do not initialise a perennial CO_2 or water ice cap in the South Pole.

We initiate a total of nine ‘pre-runs’ of the model until the global average water vapour column density and surface ice distribution reaches annual steady state, which occurs after ~ 20 Mars years. Six of these pre-runs assume two separate water radiative feedback scenarios and three North Polar Cap albedo scenarios. These two water vapour feedback scenarios are a) where atmospheric water vapour is radiatively active but water ice clouds are not; and b) where both are radiatively active. One pre-run is conducted with a North Polar Cap albedo of 0.4, where both water vapour and water ice are modelled as radiatively inactive. The final two pre-runs respectively correspond to radiatively active and inactive cloud scenarios when the South Polar CO_2 ice emissivity is set to 0.6. We then start a new set of runs with the output from the completed pre-run, where we inject engineered aerosol at a constant rate (in units of litres/s) from a specific location on the surface of Mars for 20 Mars years. These runs are listed in Table 1, and includes a 0 litre/s control where the pre-run continues for another 20 Mars years without any engineered aerosol injection. We test the sensitivity of these runs to a) the location of the aerosol release (from 0° N, 135° E by default, approximately corresponding to the coordinates of Gale Crater) and b) the dry depositional velocity of particles in the lowest layer of the atmosphere (set to 0.03 cm/s by default). Finally, we add two runs in which we inject aerosol at a constant rate for 5 Mars years, then cease aerosol release at the 5 Mars year mark (‘shutoff’) and allow the model to evolve for further 15 Mars years to study how quickly the planet reverts back to its pre-terraformed state.

A24 and R25 use finite-difference time-domain simulations to calculate the optical properties of a selection of candidate Mars-warming aerosols. However, none of these hypothetical particles have been shown to meet all the criteria for deployment on Mars, including biocompatibility (Xuan et al., 2023), manufacturability in a sustainable manner (Milligan & Elvis, 2019; Kite & Wordsworth, 2025), degradability in the Martian environment (R25), and benign interaction with spacecraft hardware (e.g. Farrell et al., 2004; Anderson et al., 2009; Barko et al., 2023). We therefore use synthetic optical constants for an idealised engineered aerosol as an input into our model, as our goal is to model the effect of artificial warming on Mars’ water cycle, not how the warming is produced.

We parametrise the optical properties of this idealised aerosol using three variables as a function of wavelength from 0.2 to 100 μm : absorption efficiency Q_{abs} (defined as the absorption cross-section of the aerosol divided by its geometric cross-section), scattering efficiency Q_{scat} (defined as the scattering cross-section of the aerosol divided by its geometric cross-section), and an asymmetry parameter $g = \{-1, 1\}$ which is equal to the integral of the cosine of the scattering phase

NPC albedo	Emissivity of South Polar CO2 ice	Radiatively active water vapour?	Radiatively active water ice clouds?	Aerosol loading (l/s) beginning t=0	Dry deposition velocity (cm/s)	Location of release (lat,lon)	Shutoff at t=... (MY)
0.35	0.747	Y	N	0	-	-	-
				2.5	0.03	(0°,135°)	-
0.35	0.747	Y	Y	0	-	-	-
				2.5	0.03	(0°,135°)	-
0.4	0.747	N	N	0	-	-	-
				2.5	0.03	(0°,135°)	-
0.4	0.747	Y	N	0	-	-	-
				1.25	0.03	(0°,135°)	-
				2.5	0.03	(0°,135°)	-
							5
				2.5	0.015	(0°,135°)	-
				2.5	0.06	(0°,135°)	-
				2.5	0.03	(-42.4°,70.5°)	-
				3.75	0.03	(0°,135°)	-
0.4	0.747	Y	Y	0	-	-	-
				2.5	0.03	(0°,135°)	-
							5
0.45	0.747	Y	N	0	-	-	-
				2.5	0.03	(-42.4°,70.5°)	-
0.45	0.747	Y	Y	0	-	-	-
				2.5	0.03	(0°,135°)	-
0.4	0.6	Y	N	0	-	-	-
				2.5	0.03	(0°,135°)	-
0.4	0.6	Y	Y	0	-	-	-
				2.5	0.03	(0°,135°)	-
							5

Table 1. List of model runs. Shared cells indicate common model starting conditions. NPC = North Polar Cap. MY = Mars Years.

function of the aerosol. Positive values of g correspond to net forward-scattering, and an isotropic scatterer has $g = 0$. We set these parameters for our idealised aerosol to share extinction trends with both the Al particle values tabulated in A24 and R25, which isotropically scatter thermal emission from the Martian surface, and the graphene-disk values in R25, which correspond to near-zero scattering, high transparency to incoming solar radiation, and strong thermal absorption (Fig. 1). We assumed a baseline extinction efficiency ($Q_{abs} + Q_{scat}$) equal to 10 across the wavelength range of analysis, and then added two Gaussian absorption peaks with a peak value of $Q_{abs} + Q_{scat} = 1000$ centred around 11 μm and 24 μm respectively and a variance of 2.5 μm (FWHM $\approx 3.7 \mu\text{m}$) to absorb the parts of the thermal emission spectrum not already absorbed by atmospheric CO_2 (which has a strong absorption peak at 15 μm). We assumed the particle was equal parts absorbing and scattering with a single-scattering albedo ($\frac{Q_{scat}}{Q_{scat}+Q_{abs}}$) equal to 0.5 at all wavelengths. Finally, we assumed a value of g to follow exponential decay with wavelength approximately corresponding to the trend seen in the asymmetry parameter of $8 \times 0.06 \times 0.06 \mu\text{m}$ Al particles (R25). We assume each aerosol particle to have a mass density of 2700 kg m^{-3} and have dimensions of $8 \times 0.06 \times 0.06 \mu\text{m}$, similar to the Al particles of R25.

3 Climate feedbacks on a warmed Mars

3.1 Global trends

In this section we focus on global average trends excluding radiative cloud feedbacks, as aerosol loadings above 2.5 l/s with radiatively active clouds lead to instabilities in the model. Under this scenario, global average temperatures approach steady state within <3 Mars years of aerosol release (Fig. 2): atmospheric engineered aerosol concentrations stabilise as the rate of removal of aerosols from the atmosphere becomes equal to the rate of release of aerosols. Steady release of 1.25 l/s, 2.5 l/s and 3.75 l/s of idealised aerosol, respectively, results in the global average surface temperature of the planet stabilising at 15 K, 25 K and 35 K above the control value of 205 K. The idealised aerosol is more potent than a realistic aerosol, being ~ 12 times more powerful than that of Al particles in R25 which are close to theoretical optima for simple shapes; our values of surface temperature with the water cycle not taken into account correspond to the results of R25 with a factor-of-12 decrease in aerosol release rates. Aerosol release causes rapid global warming proportional to the release rate. However, the aerosol lifetime, and hence the release rate that is required to maintain global heating of the surface, is very sensitive to aerosol dry deposition

velocities in the lowest layer of the atmosphere. On Earth, Brownian diffusion of particles from the atmospheric surface layer into the surface is the main surface sink of sub- μm particles (Seinfeld & Pandis, 2016; Farmer et al., 2021). However, there is no data for the dry deposition rate of sub- μm particles over desert surfaces under unstable conditions. For Mars, the dry deposition rate of sub- μm particles depends on unknowns including a) horizontal winds and turbulence close to the surface and b) surface type and roughness, and is therefore difficult to estimate *a priori* (but see Li et al., 2025 for estimates). The global average aerosol loading that can be sustained in the atmosphere is inversely proportional to the dry deposition velocity of these aerosols. A doubling of the dry deposition rate of aerosols would halve the warming for a given aerosol flux, with warming more focussed near the aerosol release point.

Although the aerosol concentration reaches steady state in <3 Mars years, water vapour continues to build up in the atmosphere for decades, which also results in greater cloud cover. In the first two Mars years of aerosol release, this is due to increased summertime sublimation from the edge of the North Polar Cap, resulting in a tenfold increase in atmospheric water vapour for every 20 K of global average surface warming. Over time, this also increases winter deposition of frost in both the Northern and Southern midlatitudes, which then sublimates in summer. This acts to even out seasonal changes in atmospheric water vapour over the course of the year. As in Vos et al. (2025), we find that the inclusion of a South Polar Cap which participates in the water cycle (which, in the case of Vos et al. (2025), is due to the effects of high obliquity as opposed to global artificial warming) results in a shift in peak humidity towards perihelion, but where seasonal sublimation from the North Polar Cap still exceeds that of the South Polar Cap. Greenhouse warming from additional water vapour causes <0.1 K change to global average surface temperature. However, once the global average amount of water ice cloud surpasses 100 precipitable μm , warming due to radiative cloud feedbacks becomes significant (Fig. 3), and global average surface temperatures increase long after the concentration of engineered aerosols has stabilised. We will elaborate on the climate impacts of this in the next subsection.

3.2 Effect of radiative cloud feedbacks on surface temperatures

Adding radiative cloud feedbacks has major effects on the water cycle (Fig. 4). The moister atmosphere caused by warming the North Polar Cap in turn results in strong cloud warming of the cap edge (which can affect the stability of the model if run over more than a decade), thereby further amplifying the seasonal sublimation of water ice from the North Polar Cap and increas-

ing water ice deposition over the South Pole. This new South Polar Cap participates in the water cycle analogously to the North Polar Cap, resulting in a water cycle that is more hemispherically and seasonally symmetric than today's cycle. This includes a shift in Aphelion Cloud Belt timing (Clancy et al., 1996) from a solar longitude (L_s) = $90^\circ - 140^\circ$ to $L_s = 60^\circ - 100^\circ$, as well as a new Perihelion Cloud Belt over the equator at $L_s = 220^\circ - 270^\circ$ caused by the movement of sublimated water vapour away from the South Pole. The Perihelion Cloud Belt is at higher altitude than the Aphelion Cloud Belt (~ 40 km) because Mars is warmer at perihelion. In contrast to the Earth, where the greenhouse effect of water vapour is significant, the Martian atmosphere still remains dry compared to that of the Earth, and so the water vapour greenhouse effect remains minor. However, when radiatively active clouds are included in the model, the clouds warm the atmosphere over the equator, suppressing cloud formation at those altitudes and allowing water vapour to ascend up into the thermosphere (>80 km altitude) during perihelion, as it does in simulations of recent Mars at high obliquity (Gilli et al., 2025). This likely accelerates atmospheric escape of water (Jakosky et al., 2018), albeit still negligibly slowly on human timescales and so is beyond the scope of this work.

Radiatively active clouds both warm and cool the surface depending on the latitude and time of day (Fig. 5). At night, clouds above 10 km altitude warm the low- and midlatitudes by up to 20 K in most seasons. During the day, thick clouds over the midlatitudes in the winter hemisphere cool the surface by up to 40 K. Frost forms at lower latitudes due to this cooling. In the Hellas Basin (Fig. 6), daytime cooling in winter can reduce day-night cycles in temperature to <5 K - remarkable given the low thermal inertia of the thin Martian atmosphere. While clouds at these latitudes cause colder winters, the ~ 5 K nighttime warming in summer lengthens the amount of time with diurnally averaged temperatures above freezing (Fig. 7). Hellas Basin warming is of particular interest in part because its relative high atmospheric pressure and shallow subsurface ice could increase its potential as a microbial habitat, if warmed (DeBenedictis et al., 2025).

Comparison to 35° obliquity simulations in the literature shows similarities and differences. Madeleine et al. (2014) and Naar (2023) find ~ 20 K warming due to radiative cloud feedbacks around the equator, with Madeleine et al. (2014) reporting globally averaged column densities of water vapour that are approximately equivalent to values we would expect for a 5 l/s aerosol loading scenario. Naar (2023) finds even greater (~ 40 - 50 K) warming in the winter-hemisphere midlatitudes, where we observe strong net cooling. Madeleine et al. (2014) find this region to be a major zone of snowfall. This suggests model intercomparisons will be required to fully assess the effects of radiatively active clouds on Mars warming.

Changing the North Polar Cap albedo (Hale et al., 2005) causes only small changes in cloud feedback strength (Fig. 7). A lower polar cap albedo causes greater water vapour sublimation in summer, and more winter cloud condensation in the midlatitudes. The North Polar Cap might darken if sublimation of bright ice leads to accumulation of darker dust, if more dust falls on the cap due to a more vigorous dust cycle (Khuller et al., 2021), or if engineered aerosol surface deposits are darker than the cap (Sagan, 1973). If polar darkening occurs, the atmosphere would moisten and might become cloudier.

3.3 Regional warming of the Hellas Basin

As liquid water could be most easily established in the Hellas Basin, it is natural to ask if engineered aerosol warming can be confined there, as it could with orbiting reflectors, but not with artificial greenhouse gas emission. This would allow limited resources to be focussed in areas where liquid water is most feasible while reducing the climate impacts elsewhere on Mars.

We find that releasing aerosols from the centre of the Hellas Basin instead of from the equator raises average summer temperatures in the Hellas Basin by 10 K (Fig. 8), despite a global reduction of aerosol density by 10% due to the increased efficiency of dry deposition in the Hellas Basin. Nonetheless, most of the aerosols disperse globally even if released from the bottom of Hellas. Thus, while warming can be focussed in the region of release, some places outside Hellas would still have summer temperatures above 273 K if no other changes were made to the release (Fig. 9), and global average temperatures would only differ by 1-3 K. The idealised aerosols studied here would therefore (for large release rates) have global effects regardless of where they were released. For real engineered aerosols, the lifetime of the aerosols in the atmosphere could be dramatically reduced by modifying particle size or density, which could confine warming.

4 Reversibility and long-term impacts of artificially warming Mars

4.1 Effect of ceasing engineered aerosol release on the climate

To test the reversibility of warming, we run two simulations (one with, and one without, radiative cloud feedbacks). In both, we set 2.5 l/s release of idealised aerosols for 5 Mars years, and then shut off the release and let the model run for another 15 Mars years. The idealised aerosols are removed by gravitational settling and dry deposition with an e-folding timescale of ~ 0.6 Mars

years. As Mars' atmosphere remains thin, and its thermal inertia low, the planet cools quickly, and the warming directly induced by the aerosols disappears after <4 Mars years (Fig. 10). However, the increased amount of ice cover means that the restoration of the Martian climate to pre-terraformed conditions is slow, taking at least decades, if not centuries (Fig. 11). This is especially true when radiative cloud feedbacks (which increase winter frost formation in the midlatitudes) are included. While the warming directly induced by the engineered aerosols disappears quickly, seasonal temperature changes due to increased cloudiness will persist for much longer, with clouds causing >20 K cooling over the winter midlatitudes that persists 15 Mars years after aerosol release stops (Fig. 12).

The size and duration of this change will depend on the duration of the initial aerosol release: the earlier the aerosol release ceases, the lower the bulk water vapour mass that would have been sublimated away from the North Polar Cap, and hence the less permanent the long-term impacts of the water cycle on seasonal temperature variation.

4.2 Surface aerosol deposition

Fig. 13 shows where engineered aerosols land on the surface. If we scale these results assuming our idealised aerosol has $12\times$ greater warming per unit mass than the Al particles in R25, then ~ 25 Mt of Al particles ($= \sim 170$ mg m⁻²) would be needed to produce the same amount of warming over 5 Mars years as for the run shown in Fig. 13, corresponding (for Al density of 2700 kg m⁻³) to a ~ 13 nm global equivalent layer of particles deposited per year. Aerosol deposition is near-uniform (whether or not radiative cloud feedbacks are included), with a small increase in deposition at lower elevations. $\sim 2\%$ of the total aerosol mass is deposited <500 km from the release site. Deposition is enhanced at the summer pole by the Hadley cell circulation acting to concentrate particles there. Over time, this could change polar cap albedo, and thus the sublimation rate of water vapour into the atmosphere. In reality, some particles would be re-lofted back into the atmosphere rather than staying on the surface, and this could extend the lifetime of aerosol warming. Alternatively, the particles may be designed to degrade into materials that are abundant on Mars. These processes would have to be quantified for real candidate warming agents using experiments in the laboratory.

4.3 Effect of Mars warming on surface water ice

The primary net source of water vapour in a warm Mars scenario is the region of perennial ice that, at the model resolution, spans latitudes between 75 and 80° N. This corresponds to a detached surface ice deposit spanning an area of approximately 100,000 sq km, separated from the main North Polar Layered Deposit by the Olympia Undae dunes region. We predict a net sublimation of 15-20 Gt/yr of water ice from this region, corresponding to ~20 cm of the topmost layer of ice per Mars year. For comparison, if we assume a net yearly accumulation of water ice on the North Polar Cap within the 0.5-1 mm/yr range predicted by models (Landis et al., 2016; Levrard et al., 2007; Hvidberg et al., 2012), this would correspond to the permanent loss of several centuries of the climate record stored in the ice deposits at 75° - 80° N every year. Water vapour sublimating from the edge of the North Polar Cap migrates towards two (and potentially three) major sinks. Firstly, winter frost thickens and spreads to lower latitudes as the atmosphere becomes more moist. This is aided by winter daytime cooling by clouds. Diurnally persistent frost in the Southern hemisphere extends up to 20°S during aphelion season, while diurnally persistent frost in the Northern hemisphere extends down to 30°N. This compares to a maximum extent down to 40° either side of the equator in the no-warming case (Fig. 14). If we neglect the radiative effects of clouds, we also find that within approximately 7 Mars years of aerosol release, most of the excess water vapour added to the Martian system by the summer sublimation of the edge of the North Polar Cap is re-deposited over the Planum Boreum (>80° N), where temperatures remain cold for a larger proportion of the year and where a moister atmosphere favours net deposition of ice. This stabilises the global-average water vapour content of the atmosphere over the year. The inclusion of radiative cloud feedbacks, however, has the opposite effect, increasing summer temperatures over Planum Boreum and causing water vapour to sublimate from the region into to the Martian atmosphere. The contribution of the Planum Boreum to the climate system in a warm Mars scenario is therefore uncertain and highly dependent on model parametrisations of cloud microphysics (see Section 5). By contrast, the trace amounts (<1 mm equivalent depth) of nighttime frost that forms atop low-latitude mountains - particularly Tharsis, Syrtis Planum and Elysium Mons - sublimates at sunrise. There is thus no migration of water towards high-altitude cold traps as proposed for Early Mars (Wordsworth et al., 2013, 2015). This is because engineered aerosol warming is more effective at low latitudes than at the poles (R25).

The final major sink of ice is at the South Pole. Approximately 100 Gt of water is seasonally exchanged between the two hemispheres within a single Mars year, with a net transfer of 5-10 Gt of water per Mars year from the Northern to the Southern hemisphere (Fig. 15). In the con-

rol case, we observe a bias in the hemispheric transfer of water of <0.1 Gt per Mars year, that is dependent on the uncertainty on the emissivity of the South Polar CO_2 cap. This bias disappears during Mars warming, as the annual deposition of water ice at the edge of the residual cap induces an albedo change that causes summer sublimation to be limited by the latent heat of water ice, thereby preventing its complete loss and gradually accumulating over latitudes polewards of 75°S to form a perennial ice cap. Each Southern summer, the northern edge of this new ice cap ($75\text{-}85^\circ\text{S}$) partially sublimates 10-20 Gt of water vapour into the atmosphere, which contributes to the water cycle as the sublimation of the edge of the North Polar Cap does in Northern Summer.

When aerosol release ceases, temperatures drop rapidly and, within a Mars year, the edge of the North Polar Cap ($75 - 80^\circ\text{N}$) is no longer a net source of water vapour in the system. Instead, the edge of the new South Polar Cap ($75 - 80^\circ\text{S}$) gradually sublimates away each summer without being replenished in winter by water sublimating off the North Polar Cap. In addition, the rapid temperature drop results in formerly seasonal frost between 65° and 75°N becoming perennial within the first 5-10 Mars years following aerosol shutoff as summer temperatures are no longer warm enough there to fully sublimate ice that accumulates there in winter. This therefore results in a reversal of hemispheric water vapour transfer, with water sublimating off the edge of the South Polar Cap and from seasonal frost in the mid-latitudes being redeposited back to the North Polar Cap, including in the region between $75 - 80^\circ\text{N}$ where approximately 15-20% of the initial ice lost is replenished. Although most of this water is permanently redeposited onto the North Polar Cap, the residual South Polar Cap also net accumulates water ice year-on-year (Fig. 16), with summer sublimation poleward of 85°S being negligible. When radiative cloud feedbacks are not taken into account, we find that ice between 80° and 85°S peaks in thickness ~ 6 Mars years after aerosol shutoff, before the cap slowly declines at a rate modulated by the assumed emissivity of the CO_2 ice deposited there (the lower the emissivity, the more rapid the sublimation). The moister atmosphere induced by radiative cloud feedbacks accelerates the accumulation of South Pole ice, and even 15 Mars years after aerosol release has ceased, latitudes poleward of 80°S continues to accumulate ice year-on-year. The water vapour content of the atmosphere plateaus 10-15 Mars years after shutoff at a new metastable equilibrium significantly moister than the pre-warming state, since the gradual sublimation of the South Polar Cap between $80 - 85^\circ\text{S}$ and, to a lesser extent, the gradual sublimation of the new perennial ice layer between 65° and 75°N , continues to supply water vapour into the atmosphere decades after aerosol release has ceased. When radiatively active clouds are accounted for, the seasonal pattern of atmospheric

water content resembles that of a recent Mars scenario without the residual South Polar CO₂ cap (Vos et al., 2025) after 15 Mars years, featuring a small spike in global water vapour content during northern summer and a larger spike during the perihelion season corresponding to the seasonal sublimation of northern and southern frost and ice respectively. Therefore, within our model framework, the change in the main surface ice reservoirs is not reversible over decadal timescales, and will continue to drive a water cycle dramatically different from that of present-day Mars for at least a century.

4.4 Effect on the CO₂ cycle

Although the winter latitudinal radius of each cap decreases by $\sim 10^\circ$ for an aerosol loading of 2.5 l/s, the increased atmospheric pressure due to the decreased global CO₂ ice deposition results in faster deposition of CO₂ ice over the winter polar cap due to an increase in the frost point of CO₂ relative to the local surface temperature. The latent heat of this extra CO₂ ice also results in surface temperatures at the poles becoming more resistant to summer warming relative to the control case, especially at the North Pole where surface CO₂ ice is modelled to have a higher albedo than at the South Pole. We observe seasonal CO₂ ice condensation in our model (Fig. 17) even in a 5 l/s aerosol loading scenario. The Martian CO₂ cycle is therefore highly robust to artificial warming by aerosols, which can create warm regions of Mars while allowing Mars to seasonally condense out its main atmospheric constituent as before - a feature that makes it unique among the eight IAU-defined planets within the Solar System (setting aside Triton and Pluto; Gao & Ohno, 2025).

4.5 Subsurface ice stability

We will now assess how warming Mars would affect the stability of subsurface ice. Warming subsurface ice could sublimate it, but this could be compensated for by an increased rate of ice formation due to the moister atmosphere. Midlatitude subsurface ice deposits have a distribution that closely corresponds to that expected for equilibrium with the modern climate (Mellon & Jakosky, 1995), but are thought to have formed under high obliquities that could take hundreds of thousands of years (Laskar et al., 2004; Smith et al., 2020; Becerra et al., 2021) to re-occur. To keep midlatitude subsurface ice deposits stable year-on-year, sublimation must be balanced by downward diffusion of water vapour back through the soil from the atmosphere - in other words, warming of the subsurface must be compensated for by an increase in humidity of the atmosphere.

Moreover, if the midlatitude deposits are to be made habitable, then some of the more accessible subsurface ice should melt seasonally, and not just sublimate or remain frozen.

Following Mellon et al. (2004) and Schörghofer and Aharonson (2005), subsurface ice of temperature $T(z)$ beneath a thickness z of permeable soil is stable when:

$$\left\langle \frac{\min(P_{surf}^{H2O}, P_{svp}^{H2O}(T_{surf}))}{T_{surf}} \right\rangle_{year} - \left\langle \frac{P_{svp}^{H2O}(T(z))}{T(z)} \right\rangle_{year} \geq 0 \quad (1)$$

where T_{surf} and P_{surf}^{H2O} are, respectively, the temperature and water vapour partial pressures at the surface, and P_{svp}^{H2O} is the saturation vapour pressure of water at temperature $T(z)$. If the first term exceeds the second term, subsurface ice will be deposited at depth z and the ice table will move toward the surface. In this study, we do not include the effect of pore space filling of soil with ice, which would increase the thermal inertia of the soil (Siegler et al., 2012; Steele et al., 2017). As a result, our model understates the stability of ice at depths <1 m in the midlatitudes relative to observed data (Dundas et al., 2018, 2021; Morgan et al., 2025).

We parametrise the stability of subsurface ice for a given soil depth z in both the pre-terraformed control case and the artificially warmed case using a single quantity, θ_z :

$$\theta_z = \text{atan2}(s_{warmed}, s_{control}) \quad (2)$$

where:

$$s = \left\langle \frac{\min(P_{surf}^{h2o}, P_{svp}^{h2o}(T_{surf}))}{T_{surf}} \right\rangle_{year} - \left\langle \frac{P_{svp}^{h2o}(T(z))}{T(z)} \right\rangle_{year} \quad (3)$$

defines the stability condition at depth z for the two respective scenarios.

The sign of $\sin(\theta_z)$ gives the net stability in the warmed case, and the sign of $\cos(\theta_z)$ provides the net stability in the control case. Therefore, it is convenient to classify our θ_z results into four separate stability scenarios: a) $0 \leq \theta_z \leq \frac{\pi}{2}$ (stable ice under both control and warmed conditions), b) $\frac{\pi}{2} \leq \theta_z \leq \pi$ (stable ice under warmed conditions, unstable ice under control conditions), c) $-\frac{\pi}{2} \leq \theta_z \leq 0$ (unstable ice under warmed conditions, stable ice under control conditions) and d) $-\pi \leq \theta_z \leq -\frac{\pi}{2}$ (unstable ice under both control and warmed conditions). We post-process MarsWRF output to assess the stability of subsurface ice, if it were present. We do not explicitly model ground ice within MarsWRF.

To calculate how fast heat is conducted through soil using MarsWRF, we divide the subsurface into 15 homogeneous layers from the surface to ~ 15 m depth, with the width of each layer increasing with depth. The thermal conductivity k_{reg} varies spatially and is derived from Mars Global Surveyor Thermal Emission Spectrometer (MGS-TES) thermal inertia data (Putzig & Mellon, 2007) assuming a uniform bulk density $\rho_{reg} = 1500 \text{ kg m}^{-3}$ and specific heat capacity $c_p = 837 \text{ J kg}^{-1} \text{ K}^{-1}$. The highest thermal conductivity values ($\sim 0.5 \text{ W m}^{-1} \text{ K}^{-1}$) are found at the poles and the lowest values ($\sim 1 \text{ mW m}^{-1} \text{ K}^{-1}$) are in dust deposits near the equator. We can define a thermal penetration depth $\approx \sqrt{\frac{k_{reg}}{c_p \rho_{reg}}} t$ where t is the duration of surface warming. Ten Mars years of engineered aerosol release corresponds to the top ~ 70 cm of the surface affected by artificial warming in low- k_{reg} soils, while in the most conductive regions the warming penetrates down to ~ 15 m. In most of Mars, however, warming would reach a depth of a few metres after 10 Mars years. Here we consider only the topmost metre of the soil. This topmost metre is the most accessible for human use, and can be probed using orbital gamma ray and neutron spectroscopy (Morgan et al., 2025).

Fig. 18 shows how subsurface ice stability shifts after 10 Mars years of artificial warming (2.5 l/s scenario, radiatively active clouds, neglecting pore closure by ice formation). Our control (0 l/s) scenario results are in line with those of Schörghofer and Aharonson (2005) for zero pore space filling, with stable subsurface ice in the topmost metre of regolith mostly confined to latitudes poleward of 60° north and south. At the poles, artificial warming acts to increase the stability of subsurface ice since the order-of-magnitude increase in surface water vapour concentration due to increased summer sublimation of water ice dominates over the increase in temperature in the shallow subsurface, which is buffered by the latent heat of the overlying ice cap. At lower latitudes, on the other hand, the increase in shallow subsurface temperatures dominates over the increase in surface humidity due to artificial warming, and so any shallow subsurface ice that exists there is rendered even less interannually stable. We also observe a hemispheric asymmetry where colder winters and more persistent surface CO_2 ice at southern high latitudes result in subsurface ice increasing in stability at the edge of the South polar ice cap following artificial warming, but decreasing at the edge of the North polar ice cap down to a depth of ~ 80 cm, although we would likely observe stable ice at shallower depths in both hemispheres if subsurface ice pore occlusion was taken into account in our model. Eventually, the water cycle will reach equilibrium, with the upper parts of the North Polar Layered Deposit and the edges of the Northern mid-latitude deposits permanently destabilised.

As warm-season average temperatures remain below freezing at latitudes with stable subsurface ice in our model, MarsWRF does not output temperatures above freezing at locations where ground ice is predicted to be stable, even in the highest aerosol loadings studied here. In reality, however, subsurface ice is observed on Mars at < 1 m depth poleward of $50\text{-}55^\circ$ latitude, including in the Southern Hellas basin (Dundas et al., 2021) where we model warm-season average temperatures of >273 K with daytime peaks >320 K. This daytime warming would sublimate any water ice within the top ~ 10 cm of soil, while deeper ice would be less sensitive to diurnal temperature forcing. The cooling effect of latent fluxes from the sublimation of water ice (Lange & Forget, 2026) is muted for subsurface ice deeper than ~ 50 cm (the level at which we estimate the evaporitic cooling rate to be equal to 10 W m^{-2} for ice sublimating at 273 K).

5 Model limitations

In this paper, we present the results of the first simulation of water cycle feedbacks on an artificially warmed Mars. However, our model is limited by a number of variables that require the following future measurements to constrain:

- Warming is sensitive to dry deposition rates for sub- μm particles, for which empirical data in Mars-like conditions is lacking.
- Maps of water ice and subsurface CO_2 remain incomplete for present-day Mars (e.g. Jakosky & Edwards, 2018; Broquet et al., 2020; Buhler & Piqueux, 2021; Jakosky & Hallis, 2024).
- We cannot predict the present-day Martian dust cycle, including large storms (Kahre, Murphy, et al., 2017). To do this requires more data on dust particles, dust lofting, and dust sources and sinks. These unknowns make it hard to know how the dust cycle would change if Mars was artificially warmed.

Ice sampling for isotopic data would be needed to quantify the water cycle feedback on temperature on Mars during historical periods of high obliquity, which still remains unknown (e.g. Mischna & Richardson, 2005) as they are highly dependent on model parametrisations of the water cycle. High-obliquity climate states of recent Mars may be the best (though imperfect) analogue to the early stages of artificial Mars warming due to the increased sublimation of water vapour induced by direct solar irradiation of the polar caps, and would therefore allow for further constraints on how the Martian climate system behaves under high atmospheric loadings of water.

Our results would also depend on a number of properties of the engineered aerosol itself, which would have to be measured experimentally. One is the ability of engineered aerosol particles to either self-agglomerate or to stick to natural dust. Another is their potential to nucleate water ice cloud particles. This could dramatically change Mars cloud properties. Because these measurements have not been conducted, we ignored them in this study, but this could lead to incorrect predictions of the effect of radiative cloud feedbacks on a warmed Mars (Madeleine et al., 2012; Navarro et al., 2014; Kahre, Haberle, et al., 2017). Aerosols settling on the surface could also change the surface albedo, and thereby alter surface temperature and/or water sublimation rate. By assuming that particles are irreversibly removed by dry deposition, we neglected other factors that might alter particle lifetime, such as (a) degradation of particles, (b) re-lofting of deposited particles, which could lead to a longer effective aerosol lifetime (analogous to that of the present-day dust cycle), and (c) agglomeration of particles causing faster sedimentation. If particles neither degrade nor agglomerate, and are easily re-lofted, then Mars would stay warm indefinitely even if particle release is cut off.

Finally, we neglected the self-stabilising effects on subsurface ice of both soil pore filling (which raises thermal inertia) and evaporitic cooling. Both effects lower peak ice temperatures and so reduce sublimation.

Even with better measurements of Mars and better lab data, there are basic limits to the predictive power of models of planetary climate change, as there are with even our best models of Earth's climate response to ongoing human-induced warming (Shaw & Stevens, 2025). As warming Mars by 30 K would be a big change to Mars' energy balance, assumptions that only apply to the modern climate might lead to incorrect extrapolations in predicting the warmed climate. Thus, any intentional alteration of Mars' surface temperature should ideally start small, start local, and be equipped with the ability to course-correct (MacMartin & Kravitz, 2019; Kite & Wordsworth, 2025). Future tests could assess if aerosol warming can be confined to a small topographic basin, for instance, by releasing aerosol particles from the centre of the Hellas Basin that are engineered to have a short lifetime in the atmosphere that does not allow global dispersal.

In summary, processes left unaccounted for in existing models of a warmed Mars could lead to undesirable outcomes. We do not yet know whether warming Mars would permit a new biosphere or aid human exploration. Thus, more data (including, but not limited to, Mars sample return) is needed about Mars to enable informed decisions about the role of humans in Mars'

future and the possibility of permanent inhabitation (Kite & Wordsworth, 2025; National Academies of Sciences, Engineering, and Medicine, 2025).

5.1 Conclusions

In principle, Mars might be warmed using aerosols (Ansari et al., 2024), gases (Marinova et al., 2005), or solar reflectors (Handmer, 2024). However, the costs, benefits, and possible risks of warming Mars remain unclear. Previous work neglected the effects of warming on the Mars water cycle, whose radiative impacts could accelerate or delay warming, and move ice to high-altitude zones that are unfavorable for melting. We modelled the effect on the water cycle of the release of an engineered aerosol with idealised Mars-warming radiative properties into Mars' atmosphere, neglecting microphysical interactions between aerosols. Within our model framework, we found that a warmer Mars results in a moister atmosphere, with strong radiative cloud feedbacks: nighttime warming over most of the planet, and strong daytime cooling in the winter mid-latitudes. Water ice is slowly lost from surface and subsurface reservoirs near the North Pole, and accumulates over the South Pole. This causes a positive feedback where seasonal sublimation from the South Polar Cap contributes more to the water cycle, boosting the amount of atmospheric water vapour and clouds (see Fig. 19 for a graphical summary). In turn, this boosts radiative cloud feedbacks, warming most of Mars but with strong winter cooling over the midlatitudes. The effects of this change in the water cycle persist for at least decades even if aerosol release is ended, as the long-term redistribution of ice towards the South Pole causes winter radiative cloud feedbacks to cause strong cooling in both the Northern and Southern mid-latitudes, increasing the formation of winter frost that acts as an additional major reservoir of ice in the Martian climate system.

In closing, we emphasise that, even if Mars' surface can be warmed, the planet would still remain a much more hostile environment than the Earth for even the hardiest life forms, let alone humans, and no known extremophile can tolerate all of the stresses of the Martian environment (Coleine et al., 2025; DeBenedictis et al., 2025). Mars lacks a breathable atmosphere and an effective shield against harmful UV radiation, while its soil is salty and contains perchlorates that can inhibit plant growth. Warming Mars will therefore not be a substitute for protecting the environment of the only habitable planet we will have for the foreseeable future (the Earth), while changing the Martian environment in ways that could take at least decades to reverse.

Acknowledgments

This work was partly funded by a Residency for E.S.K at Astera Institute. This work used resources from the University of Chicago's Research Computing Center and the NASA High-End Computing (HEC) Program through the NASA Advanced Supercomputing (NAS) Division at Ames Research Center. A portion of this work was conducted at the Jet Propulsion Laboratory, California Institute of Technology, under contract with NASA. We thank the PlanetWRF development team for their support.

Open access statement:

All model output is available on Zenodo (doi:10.5281/zenodo.18717694), including input files that allow for reproducibility of all of the figures presented here. Requests for the MarsWRF source code should be submitted to mir@aeolisresearch.com.

References

- Aharonson, O., Vos, E., Millour, E., Forget, F., & Schörghofer, N. (2026). Milankovitch forcing of equilibrium ground-ice on Mars. *Icarus*, *444*, 116772. doi: <https://doi.org/10.1016/j.icarus.2025.116772>
- Anderson, R. C., Beegle, L. W., Peters, G. H., Fleming, G. M., Jandura, L., Kriechbaum, K., ... Sunshine, D. (2009). Particle transport and distribution on the Mars Science Laboratory mission: Effects of triboelectric charging. *Icarus*, *204*, 545-557. doi: [10.1016/j.icarus.2009.07.006](https://doi.org/10.1016/j.icarus.2009.07.006)
- Ansari, S., Kite, E. S., Ramirez, R., Steele, L. J., & Mohseni, H. (2024). Feasibility of keeping Mars warm with nanoparticles. *Sci. Adv.*, *10*, eadn4650. doi: [10.1126/sciadv.adn4650](https://doi.org/10.1126/sciadv.adn4650)
- Atwood, S. A., Smith, M. D., Wolff, M. J., Badri, K., Edwards, C. S., Christensen, P. R., ... El-Maarry, M. R. (2024, August). Spatial and temporal variability of martian water-ice cloud effective radius in EMIRS thermal infrared observations. *Icarus*, *418*, 116148. doi: [10.1016/j.icarus.2024.116148](https://doi.org/10.1016/j.icarus.2024.116148)
- Bapst, J., Bandfield, J. L., & Wood, S. E. (2015). Hemispheric asymmetry in martian seasonal surface water ice from MGS TES. *Icarus*, *260*, 396-408. doi: [10.1016/j.icarus.2015.07.025](https://doi.org/10.1016/j.icarus.2015.07.025)
- Barko, G., Kalacska, G., Keresztes, R., Zsidai, L., Shegawu, H., & Kalacska, A. (2023).

- Abrasion Evaluation of Moon and Mars Simulants on Rotating Shaft/Sealing Materials: Simulants and Structural Materials Review and Selection. *Lubricants*, 11(8). doi: 10.3390/lubricants11080334
- Becerra, P., Bramson, A., Brown, A., Byrne, S., Coronato, A., Diniega, S., ... others (2021). The Importance of the Climate Record in the Martian Polar Layered Deposits. In *BAAS* (Vol. 53, p. 144). doi: 10.3847/25c2cfef.90c37f59
- Bramson, A., Andres, C., Bapst, J., Becerra, P., Courville, S. W., Dundas, C. M., ... others (2021). Mid-Latitude Ice on Mars: A Science Target for Planetary Climate Histories and an Exploration Target for In Situ Resources. In *BAAS* (Vol. 53, p. 115). doi: 10.3847/25c2cfef.cc90422d
- Broquet, A., Wieczorek, M. A., & Fa, W. (2020). Flexure of the Lithosphere Beneath the North Polar Cap of Mars: Implications for Ice Composition and Heat Flow. *Geophys. Res. Lett.*, 47, e86746. doi: 10.1029/2019GL08674610.1002/essoar.10501496.1
- Buhler, P. B., Ingersoll, A. P., Piqueux, S., Ehlmann, B. L., & Hayne, P. O. (2020). Coevolution of Mars's atmosphere and massive south polar CO₂ ice deposit. *Nat. Astron.*, 4, 364-371. doi: 10.1038/s41550-019-0976-8
- Buhler, P. B., & Piqueux, S. (2021). Obliquity Driven CO₂ Exchange Between Mars' Atmosphere, Regolith, and Polar Cap. *J. Geophys. Res. Planets*, 126, e06759. doi: 10.1029/2020JE006759
- Carr, M. H., & Head, J. W. (2015). Martian surface/near-surface water inventory: Sources, sinks, and changes with time. *Geophys. Res. Lett.*, 42(3), 726-732. doi: 10.1002/2014GL062464
- Clancy, R. T., Grossman, A. W., Wolff, M. J., James, P. B., Rudy, D. J., Billawala, Y. N., ... Muhleman, D. O. (1996). Water Vapor Saturation at Low Altitudes around Mars Aphelion: A Key to Mars Climate? *Icarus*, 122, 36-62. doi: 10.1006/icar.1996.0108
- Colaprete, A., Barnes, J. R., Haberle, R. M., Hollingsworth, J. L., Kieffer, H. H., & Titus, T. N. (2005). Albedo of the south pole on Mars determined by topographic forcing of atmosphere dynamics. *Nature*, 435, 184-188. doi: 10.1038/nature03561
- Coleine, C., Delgado-Baquerizo, M., Rosado, A. S., & Zerbini, A. (2025). The role of extremophile microbiomes in terraforming Mars. *Communications Biology*, 8, 1588. doi: 10.1038/s42003-025-08973-1
- Craddock, R. A., & Howard, A. D. (2002). The case for rainfall on a warm, wet early Mars.

- J. Geophys. Res. Planets*, 107, 5111. doi: 10.1029/2001JE001505
- DeBenedictis, E. A., Kite, E. S., Wordsworth, R. D., Lanza, N. L., Cockell, C. S., Silver, P. A., ... McKay, C. P. (2025). The case for Mars terraforming research. *Nat. Astron.*, 9, 634-639. doi: 10.1038/s41550-025-02548-0
- Dicaire, I., Forget, F., Millour, E., Maan, D. C., Nachon, M., & Summerer, L. (2013). Using Martian Climate Models to assess the Potential of Artificial Greenhouse Gases to increase Martian Surface Temperatures. In *Proceedings 64th international astronomical congress, iac13*.
- Dundas, C. M., Bramson, A. M., Ojha, L., Wray, J. J., Mellon, M. T., Byrne, S., ... Holt, J. W. (2018). Exposed subsurface ice sheets in the Martian mid-latitudes. *Science*, 359, 199-201. doi: 10.1126/science.aao1619
- Dundas, C. M., Mellon, M. T., Conway, S. J., Daubar, I. J., Williams, K. E., Ojha, L., ... Pathare, A. V. (2021). Widespread Exposures of Extensive Clean Shallow Ice in the Midlatitudes of Mars. *J. Geophys. Res. Planets*, 126, e06617. doi: 10.1029/2020JE006617
- Farmer, D. K., Boedicker, E. K., & DeBolt, H. M. (2021). Dry deposition of atmospheric aerosols: Approaches, observations, and mechanisms. *Annual review of physical chemistry*, 72, 375-397. doi: 10.1146/annurev-physchem-090519-034936
- Farrell, W. M., Smith, P. H., Delory, G. T., Hillard, G. B., Marshall, J. R., Catling, D., ... Johnson, B. (2004). Electric and magnetic signatures of dust devils from the 2000-2001 MATADOR desert tests. *J. Geophys. Res. Planets*, 109, E03004. doi: 10.1029/2003JE002088
- Forget, F., Barthomeuf, P., Sivula, O., Freissinet, C., Lee, N. M., Mangold, N., ... Tønnessen, M. (2024). Mars as a Planet B? In C. Verseux, M. Gargaud, K. Lehto, & M. Viso (Eds.), *Mars and the Earthlings: A Realistic View on Mars Exploration and Settlement* (pp. 341–366). Springer Nature Switzerland. doi: 10.1007/978-3-031-66881-4_9
- Forget, F., Haberle, R. M., Montmessin, F., Levrard, B., & Head, J. W. (2006). Formation of Glaciers on Mars by Atmospheric Precipitation at High Obliquity. *Science*, 311, 368-371. doi: 10.1126/science.1120335
- Forni, O., Gaft, M., Toplis, M. J., Clegg, S. M., Maurice, S., Wiens, R. C., ... others (2015). First detection of fluorine on Mars: Implications for Gale Crater's geochemistry. *Geophys. Res. Lett.*, 42, 1020-1028. doi: 10.1002/2014GL062742

- Gao, P., & Ohno, K. (2025). Clouds and Hazes in the Atmospheres of Triton and Pluto. In A. Luspay-Kuti & K. Mandt (Eds.), *Triton and Pluto; The long lost twins of active worlds* (p. 6-1). doi: 10.1088/2514-3433/ad5278ch6
- Gary-Bicas, C. E., Hayne, P. O., Horvath, T., Heavens, N. G., Kass, D. M., Kleinböhl, A., ... McCleese, D. J. (2020). Asymmetries in Snowfall, Emissivity, and Albedo of Mars' Seasonal Polar Caps: Mars Climate Sounder Observations. *J. Geophys. Res. Planets*, *125*, e06150. doi: 10.1029/2019JE006150
- Gerstell, M. F., Francisco, J. S., Yung, Y. L., Boxe, C., & Aaltonee, E. T. (2001). Keeping mars warm with new super greenhouse gases. *Proc. Natl. Acad. Sci. U.S.A.*, *98*, 2154-2157. doi: 10.1073/pnas.051511598
- Gilli, G., González-Galindo, F., Chaufray, J.-Y., Millour, E., Forget, F., Montmessin, F., ... Brines, A. (2025). Increased hydrogen escape from Mars atmosphere during periods of high obliquity. *Nat. Astron.*, *9*, 960-968. doi: 10.1038/s41550-025-02561-3
- Grimm, R. E., Harrison, K. P., Stillman, D. E., & Kirchoff, M. R. (2017). On the secular retention of ground water and ice on Mars. *J. Geophys. Res. Planets*, *122*, 94-109. doi: 10.1002/2016JE005132
- Guo, X., Lawson, W. G., Richardson, M. I., & Toigo, A. (2009). Fitting the Viking lander surface pressure cycle with a Mars General Circulation Model. *J. Geophys. Res. Planets*, *114*, E07006. doi: 10.1029/2008JE003302
- Haberle, R. M. (2013). Estimating the power of Mars' greenhouse effect. *Icarus*, *223*, 619-620. doi: 10.1016/j.icarus.2012.12.022
- Haberle, R. M., Kahre, M. A., Hollingsworth, J. L., Montmessin, F., Wilson, R. J., Urata, R. A., ... Schaeffer, J. R. (2019). Documentation of the NASA/Ames Legacy Mars Global Climate Model: Simulations of the present seasonal water cycle. *Icarus*, *333*, 130-164. doi: 10.1016/j.icarus.2019.03.026
- Haberle, R. M., Murphy, J. R., & Schaeffer, J. (2003). Orbital change experiments with a Mars general circulation model. *Icarus*, *161*, 66-89. doi: 10.1016/S0019-1035(02)00017-9
- Hale, A. S., Bass, D. S., & Tamppari, L. K. (2005). Monitoring the perennial Martian northern polar cap with MGS MOC. *Icarus*, *174*, 502-512. doi: 10.1016/j.icarus.2004.10.033
- Handmer, C. J. (2024). How to Terraform Mars for \$50B with Solar Sails. In *Tenth International Conference on Mars* (Vol. 3007, p. 3025).

- Haqq-Misra, J. (2012, October). An Ecological Compass for Planetary Engineering. *Astrobiology*, *12*, 985-997. doi: 10.1089/ast.2011.0796
- Hoffman, J. A., Hecht, M. H., Rapp, D., Hartvigsen, J. J., SooHoo, J. G., Aboobaker, A. M., ... others (2022). Mars Oxygen ISRU Experiment (MOXIE)—Preparing for human Mars exploration. *Sci. Adv.*, *8*, eabp8636. doi: 10.1126/sciadv.abp8636
- Hvidberg, C. S., Fishbaugh, K. E., Winstrup, M., Svensson, A., Byrne, S., & Herkenhoff, K. E. (2012). Reading the climate record of the martian polar layered deposits. *Icarus*, *221*, 405-419. doi: 10.1016/j.icarus.2012.08.009
- Hynek, B. M., Beach, M., & Hoke, M. R. T. (2010). Updated global map of Martian valley networks and implications for climate and hydrologic processes. *J. Geophys. Res. Planets*, *115*, E09008. doi: 10.1029/2009JE003548
- Ingersoll, A. P. (1970). Mars: Occurrence of Liquid Water. *Science*, *168*, 972-973. doi: 10.1126/science.168.3934.972
- Iwabuchi, H., & Yang, P. (2011). Temperature dependence of ice optical constants: Implications for simulating the single-scattering properties of cold ice clouds. *J. Quant. Spec. Radiat. Transf.*, *112*, 2520-2525. doi: 10.1016/j.jqsrt.2011.06.017
- Jakosky, B. M. (2024). Mars' atmosphere, volatiles, and climate as the sun heats up over the next 6 billion years. *Icarus*, *410*, 115888. doi: 10.1016/j.icarus.2023.115888
- Jakosky, B. M., Brain, D., Chaffin, M., Curry, S., Deighan, J., Grebowsky, J., ... others (2018). Loss of the Martian atmosphere to space: Present-day loss rates determined from MAVEN observations and integrated loss through time. *Icarus*, *315*, 146-157. doi: 10.1016/j.icarus.2018.05.030
- Jakosky, B. M., & Edwards, C. S. (2018). Inventory of CO₂ available for terraforming Mars. *Nat. Astron.*, *2*, 634-639. doi: 10.1038/s41550-018-0529-6
- Jakosky, B. M., & Hallis, L. J. (2024). Fate of an Earth-Like Water Inventory on Mars. *J. Geophys. Res. Planets*, *129*, e2023JE008159. doi: 10.1029/2023JE008159
- James, P. B., Cantor, B. A., & Davis, S. (2001). Mars Orbiter Camera observations of the Martian south polar cap in 1999-2000. *J. Geophys. Res.*, *106*, 23635-23652. doi: 10.1029/2000JE001313
- James, P. B., Thomas, P. C., Wolff, M. J., & Bonev, B. P. (2007). MOC observations of four Mars year variations in the south polar residual cap of Mars. *Icarus*, *192*, 318-326. doi: 10.1016/j.icarus.2007.07.014
- Kahre, M. A., Haberle, R. M., Hollingsworth, J. L., Montmessin, F., Brecht, A. S., Urata, R.,

- ... Wolff, M. J. (2017). Updates on Modeling the Water Cycle with the NASA Ames Mars Global Climate Model. In F. Forget & M. Millour (Eds.), *The Mars Atmosphere: Modelling and observation* (p. 3209).
- Kahre, M. A., Murphy, J. R., Newman, C. E., Wilson, R. J., Cantor, B. A., Lemmon, M. T., & Wolff, M. J. (2017). The Mars Dust Cycle. In R. M. Haberle, R. T. Clancy, F. Forget, M. D. Smith, & R. W. Zurek (Eds.), *The Atmosphere and Climate of Mars* (p. 229-294). doi: 10.1017/9781139060172.010
- Khuller, A. R., Christensen, P. R., & Warren, S. G. (2021). Spectral Albedo of Dusty Martian H₂O Snow and Ice. *J. Geophys. Res. Planets*, *126*, e06910. doi: 10.1029/2021JE006910
- Khuller, A. R., & Clow, G. D. (2024). Turbulent Fluxes and Evaporation/Sublimation Rates on Earth, Mars, Titan, and Exoplanets. *J. Geophys. Res. Planets*, *129*, e2023JE008114. doi: 10.1029/2023JE008114
- Kite, E., & Wordsworth, R. (2025). Greening the solar system. *Asterisk Magazine*, *9*, 114-122.
- Kite, E. S., & Conway, S. (2024). Geological evidence for multiple climate transitions on Early Mars. *Nat. Geosci.*, *17*, 10-19. doi: 10.1038/s41561-023-01349-2
- Kite, E. S., Steele, L. J., Mischna, M. A., & Richardson, M. I. (2021, May). Warm early Mars surface enabled by high-altitude water ice clouds. *Proc. Natl. Acad. Sci. U.S.A.*, *118*, e2101959118. doi: 10.1073/pnas.2101959118
- Kutepov, A., Feofilov, A., Rezac, L., & Kalogerakis, K. S. (2025). Remote Sensing in the 15 μ m CO₂ Band: Key Concepts and Implications for the Heat Balance of Mesosphere and Thermosphere. *Remote Sens.*, *17*. doi: 10.3390/rs17111896
- Landis, M. E., Byrne, S., Daubar, I. J., Herkenhoff, K. E., & Dundas, C. M. (2016). A revised surface age for the North Polar Layered Deposits of Mars. *Geophys. Res. Lett.*, *43*, 3060-3068. doi: 10.1002/2016GL068434
- Lange, L., & Forget, F. (2026). On the Possibility of Melting Water Ice during the Recent Past of Mars. Implications for the Formation of Gullies. *J. Geophys. Res. Planets*, *131*, e2025JE009512. doi: 10.1029/2025JE009512
- Lange, L., Piqueux, S., Edwards, C. S., Forget, F., Naar, J., Vos, E., & Szantai, A. (2024). Observations of Water Frost on Mars With THEMIS: Application to the Presence of Brines and the Stability of (Sub)Surface Water Ice. *J. Geophys. Res. Planets*, *129*, e2024JE008489. doi: 10.1029/2024JE008489

- Laskar, J., Correia, A. C. M., Gastineau, M., Joutel, F., Levrard, B., & Robutel, P. (2004). Long term evolution and chaotic diffusion of the insolation quantities of Mars. *Icarus*, *170*, 343-364. doi: 10.1016/j.icarus.2004.04.005
- Lee, C., Richardson, M. I., Newman, C. E., & Mischna, M. A. (2018). The sensitivity of solsticial pauses to atmospheric ice and dust in the MarsWRF General Circulation Model. *Icarus*, *311*, 23-34. doi: 10.1016/j.icarus.2018.03.019
- Leighton, R. B., & Murray, B. C. (1966). Behavior of carbon dioxide and other volatiles on mars. *Science*, *153*, 136-144. doi: 10.1126/science.153.3732.136
- Levrard, B., Forget, F., Montmessin, F., & Laskar, J. (2004). Recent ice-rich deposits formed at high latitudes on Mars by sublimation of unstable equatorial ice during low obliquity. *Nature*, *431*, 1072-1075. doi: 10.1038/nature03055
- Levrard, B., Forget, F., Montmessin, F., & Laskar, J. (2007). Recent formation and evolution of northern Martian polar layered deposits as inferred from a Global Climate Model. *J. Geophys. Res. Planets*, *112*, E06012. doi: 10.1029/2006JE002772
- Li, L., Zhao, C., Newman, C. E., Zhao, Y., Feng, J., Li, T., ... Yue, Y. (2025). Impacts of Dry Deposition Processes With Resolved Dust Particle Sizes on Simulating the Martian Dust. *J. Geophys. Res. Planets*, *130*, e2024JE008616. doi: 10.1029/2024JE008616
- MacMartin, D. G., & Kravitz, B. (2019). The engineering of climate engineering. *Annual Review of Control, Robotics, and Autonomous Systems*, *2*, 445-467. doi: <https://doi.org/10.1146/annurev-control-053018-023725>
- Madeleine, J. B., Forget, F., Head, J. W., Levrard, B., Montmessin, F., & Millour, E. (2009). Amazonian northern mid-latitude glaciation on Mars: A proposed climate scenario. *Icarus*, *203*, 390-405. doi: 10.1016/j.icarus.2009.04.037
- Madeleine, J.-B., Forget, F., Millour, E., Navarro, T., & Spiga, A. (2012). The influence of radiatively active water ice clouds on the Martian climate. *Geophys. Res. Lett.*, *39*, L23202. doi: 10.1029/2012GL053564
- Madeleine, J.-B., Head, J. W., Forget, F., Navarro, T., Millour, E., Spiga, A., ... Dickson, J. L. (2014). Recent Ice Ages on Mars: The role of radiatively active clouds and cloud microphysics. *Geophys. Res. Lett.*, *41*, 4873-4879. doi: 10.1002/2014GL059861
- Marinova, M. M., McKay, C. P., & Hashimoto, H. (2005). Radiative-convective model of warming Mars with artificial greenhouse gases. *J. Geophys. Res. Planets*, *110*, E03002. doi: 10.1029/2004JE002306

- Marshall, A. (1993). Ethics and the extraterrestrial environment. *Journal of Applied Philosophy*, *10*, 227–236.
- McKay, C. P., Toon, O. B., & Kasting, J. F. (1991). Making Mars habitable. *Nature*, *352*, 489–496. doi: 10.1038/352489a0
- Mellon, M. T., Feldman, W. C., & Prettyman, T. H. (2004). The presence and stability of ground ice in the southern hemisphere of Mars. *Icarus*, *169*, 324–340. doi: 10.1016/j.icarus.2003.10.022
- Mellon, M. T., & Jakosky, B. M. (1995). The distribution and behavior of Martian ground ice during past and present epochs. *J. Geophys. Res.*, *100*, 11781–11799.
- Michalakes, J., Dudhia, J., Gill, D., Henderson, T., Klemp, J., Skamarock, W., & Wang, W. (2004). The Weather Research and Forecast Model: Software Architecture and Performance. In *Use of high performance computing in meteorology* (p. 156–168). doi: 10.1142/9789812701831_0012
- Milligan, T., & Elvis, M. (2019). Mars Environmental Protection: An Application of the 1/8 Principle. In K. Szocik (Ed.), *The human factor in a mission to mars* (p. 167). doi: 10.1007/978-3-030-02059-0_10
- Mischna, M. A., Lee, C., & Richardson, M. (2012). Development of a fast, accurate radiative transfer model for the Martian atmosphere, past and present. *J. Geophys. Res. Planets*, *117*, E10009. doi: 10.1029/2012JE004110
- Mischna, M. A., & Richardson, M. I. (2005). A reanalysis of water abundances in the Martian atmosphere at high obliquity. *Geophys. Res. Lett.*, *32*, L03201. doi: 10.1029/2004GL021865
- Mischna, M. A., Richardson, M. I., Wilson, R. J., & McCleese, D. J. (2003). On the orbital forcing of Martian water and CO₂ cycles: A general circulation model study with simplified volatile schemes. *J. Geophys. Res. Planets*, *108*, 5062. doi: 10.1029/2003JE002051
- Mondro, C. A., Grotzinger, J., Fedo, C. M., Lamb, M. P., Gupta, S., Dietrich, W. E., . . . others (2025). Depositional Environment of the Amapari Marker Band: Rising Water Levels Formed Kilometer-Scale Lake in Gale Crater, Mars. *J. Geophys. Res. Planets*, *130*, 2024JE008606. doi: 10.1029/2024JE008606
- Montabone, L., Forget, F., Millour, E., Wilson, R. J., Lewis, S. R., Cantor, B., . . . Wolff, M. J. (2015). Eight-year climatology of dust optical depth on Mars. *Icarus*, *251*, 65–95. doi: 10.1016/j.icarus.2014.12.034

- Montabone, L., Spiga, A., Kass, D. M., Kleinböhl, A., Forget, F., & Millour, E. (2020). Martian Year 34 Column Dust Climatology from Mars Climate Sounder Observations: Reconstructed Maps and Model Simulations. *J. Geophys. Res. Planets*, *125*, e06111. doi: 10.1029/2019JE006111
- Montmessin, F., Smith, M. D., Langevin, Y., Mellon, M. T., & Fedorova, A. (2017). The Water Cycle. In R. M. Haberle, R. T. Clancy, F. Forget, M. D. Smith, & R. W. Zurek (Eds.), *The Atmosphere and Climate of Mars* (p. 295-337). doi: 10.1017/9781139060172.011
- Morgan, G. A., Putzig, N. E., Baker, D. M. H., Pathare, A., Dundas, C. M., Russell, M. B., ... Bain, Z. (2025). Refined Mapping of Subsurface Water Ice on Mars to Support Future Missions. *Planet. Sci.*, *6*, 29. doi: 10.3847/PSJ/ad9b24
- Naar, J. (2023). *Modélisation du cycle de l'eau actuel et des derniers âges glaciaires de la planète mars*. (Doctoral dissertation, Sorbonne Université). doi: 10.13140/RG.2.2.31506.84162
- National Academies of Sciences, Engineering, and Medicine. (2025). *A science strategy for the human exploration of mars*. The National Academies Press. doi: 10.17226/28594
- Navarro, T., Madeleine, J.-B., Forget, F., Spiga, A., Millour, E., Montmessin, F., & Määttänen, A. (2014). Global climate modeling of the Martian water cycle with improved microphysics and radiatively active water ice clouds. *J. Geophys. Res. Planets*, *119*, 1479-1495. doi: 10.1002/2013JE004550
- Pommerol, A., Portyankina, G., Thomas, N., Aye, K.-M., Hansen, C. J., Vincendon, M., & Langevin, Y. (2011). Evolution of south seasonal cap during Martian spring: Insights from high-resolution observations by HiRISE and CRISM on Mars Reconnaissance Orbiter. *J. Geophys. Res. Planets*, *116*, E08007. doi: 10.1029/2010JE003790
- Putzig, N. E., & Mellon, M. T. (2007). Apparent thermal inertia and the surface heterogeneity of Mars. *Icarus*, *191*, 68-94. doi: 10.1016/j.icarus.2007.05.013
- Rampe, E. B., Cartwright, J. A., McCubbin, F. M., & Osterloo, M. M. (2018). The role of halogens during fluid and magmatic processes on mars. In *The Role of Halogens in Terrestrial and Extraterrestrial Geochemical Processes: Surface, Crust, and Mantle* (pp. 959-995). Springer.
- Richardson, M. I., Ansari, S., Fan, B., Ramirez, R., Mohseni, H., Mischna, M. A., ... Kite, E. S. (2025). *Atmospheric dynamics of first steps toward terraforming Mars*. Retrieved from <https://arxiv.org/abs/2504.01455>

- Richardson, M. I., Toigo, A. D., & Newman, C. E. (2007). PlanetWRF: A general purpose, local to global numerical model for planetary atmospheric and climate dynamics. *J. Geophys. Res. Planets*, *112*, E09001. doi: 10.1029/2006JE002825
- Sagan, C. (1973). Planetary Engineering on Mars. *Icarus*, *20*, 513-514. doi: 10.1016/0019-1035(73)90026-2
- Schmidt, F., Douté, S., Schmitt, B., Vincendon, M., Bibring, J.-P., Langevin, Y., & Omega Team. (2009). Albedo control of seasonal South Polar cap recession on Mars. *Icarus*, *200*, 374-394. doi: 10.1016/j.icarus.2008.12.014
- Schörghofer, N. (2020). Mars: Quantitative Evaluation of Crocus Melting behind Boulders. *ApJ*, *890*, 49. doi: 10.3847/1538-4357/ab612f
- Schörghofer, N., & Aharonson, O. (2005). Stability and exchange of subsurface ice on Mars. *J. Geophys. Res. Planets*, *110*, E05003. doi: 10.1029/2004JE002350
- Schörghofer, N., & Forget, F. (2012). History and anatomy of subsurface ice on mars. *Icarus*, *220*, 1112-1120. doi: <https://doi.org/10.1016/j.icarus.2012.07.003>
- Schwartz, J. S. J. (2013). On the moral permissibility of terraforming. *Ethics Environ.*, *18*(2), 1–31.
- Seinfeld, J. H., & Pandis, S. N. (2016). *Atmospheric Chemistry and Physics: From Air Pollution to Climate Change* (3rd ed.). John Wiley and Sons.
- Shaw, T., & Stevens, B. (2025). The other climate crisis. *Nature*, *639*, 877-887. doi: 10.1038/s41586-025-08680-1
- Siegler, M., Aharonson, O., Carey, E., Choukroun, M., Hudson, T., Schörghofer, N., & Xu, S. (2012). Measurements of thermal properties of icy Mars regolith analogs. *J. Geophys. Res. Planets*, *117*, E03001. doi: 10.1029/2011JE003938
- Skamarock, W. C., Klemp, J. B., Dudhia, J., Gill, D. O., Barker, D. M., Wang, W., & Powers, J. G. (2005). A Description of the Advanced Research WRF Version 2.. doi: 10.5065/D6DZ069T
- Smith, I. B., Hayne, P. O., Byrne, S., Becerra, P., Kahre, M., Calvin, W., . . . others (2020). The Holy Grail: A road map for unlocking the climate record stored within Mars' polar layered deposits. *Planet. Space Sci.*, *184*, 104841. doi: 10.1016/j.pss.2020.104841
- Steele, L. J., Balme, M. R., & Lewis, S. R. (2017). Regolith-atmosphere exchange of water in Mars' recent past. *Icarus*, *284*, 233-248. doi: 10.1016/j.icarus.2016.11.023
- Stoner, I. (2021). The ethics of terraforming: A critical survey of six arguments. In *Terraforming mars* (p. 99-115). John Wiley and Sons, Ltd. doi: <https://doi.org/10.1002/>

9781119761990.ch6

- Streeter, P. M., Lewis, S. R., Patel, M. R., Holmes, J. A., & Kass, D. M. (2020). Surface Warming During the 2018/Mars Year 34 Global Dust Storm. *Geophys. Res. Lett.*, *47*, e83936. doi: 10.1029/2019GL083936
- Toigo, A. D., Lee, C., Newman, C. E., & Richardson, M. I. (2012). The impact of resolution on the dynamics of the martian global atmosphere: Varying resolution studies with the MarsWRF GCM. *Icarus*, *221*, 276-288. doi: 10.1016/j.icarus.2012.07.020
- Vos, E., Aharonson, O., & Forget, F. (2025). Mars Without the Southern Perennial CO₂ Cover. *Geophys. Res. Lett.*, *52*, 2024GL113274. doi: 10.1029/2024GL113274
- Williams, R. J., McKay, D. S., Giles, D., & Bunch, T. E. (1979). Mining and Beneficiation of Lunar Ores. In G. K. O'Neill, J. Billingham, W. Gilbreath, B. O'Leary, & B. Gossett (Eds.), *NASA Special Publication* (Vol. 428, p. 275).
- Wilson, R. J., Neumann, G. A., & Smith, M. D. (2007). Diurnal variation and radiative influence of Martian water ice clouds. *Geophys. Res. Lett.*, *34*, L02710. doi: 10.1029/2006GL027976
- Wolff, M. J., Smith, M. D., Clancy, R. T., Arvidson, R., Kahre, M., Seelos, F., . . . Savijärvi, H. (2009). Wavelength dependence of dust aerosol single scattering albedo as observed by the Compact Reconnaissance Imaging Spectrometer. *J. Geophys. Res. Planets*, *114*, E00D04. doi: 10.1029/2009JE003350
- Wordsworth, R., & Cockell, C. (2024). Self-Sustaining Living Habitats in Extraterrestrial Environments. *Astrobiology*, *24*, 1187-1195. doi: 10.1089/ast.2024.0080
- Wordsworth, R., Forget, F., Millour, E., Head, J. W., Madeleine, J. B., & Charnay, B. (2013). Global modelling of the early martian climate under a denser CO₂ atmosphere: Water cycle and ice evolution. *Icarus*, *222*, 1-19. doi: 10.1016/j.icarus.2012.09.036
- Wordsworth, R., Kerber, L., & Cockell, C. (2019). Enabling Martian habitability with silica aerogel via the solid-state greenhouse effect. *Nat. Astron.*, *3*, 898-903. doi: 10.1038/s41550-019-0813-0
- Wordsworth, R., Kerber, L., Pierrehumbert, R. T., Forget, F., & Head, J. W. (2015). Comparison of “warm and wet” and “cold and icy” scenarios for early Mars in a 3-D climate model. *J. Geophys. Res. Planets*, *120*, 1201-1219. doi: 10.1002/2015JE004787
- Xuan, L., Ju, Z., Skonieczna, M., Zhou, P. K., & Huang, R. (2023). Nanoparticles-induced potential toxicity on human health: Applications, toxicity mechanisms, and evaluation models. *MedComm.*, *4*, e327. doi: 10.1002/mco2.327

Zubrin, R. M., & McKay, C. P. (1997). Technological requirements for terraforming Mars.
J. Br. Interplanet. Soc., 50, 309.

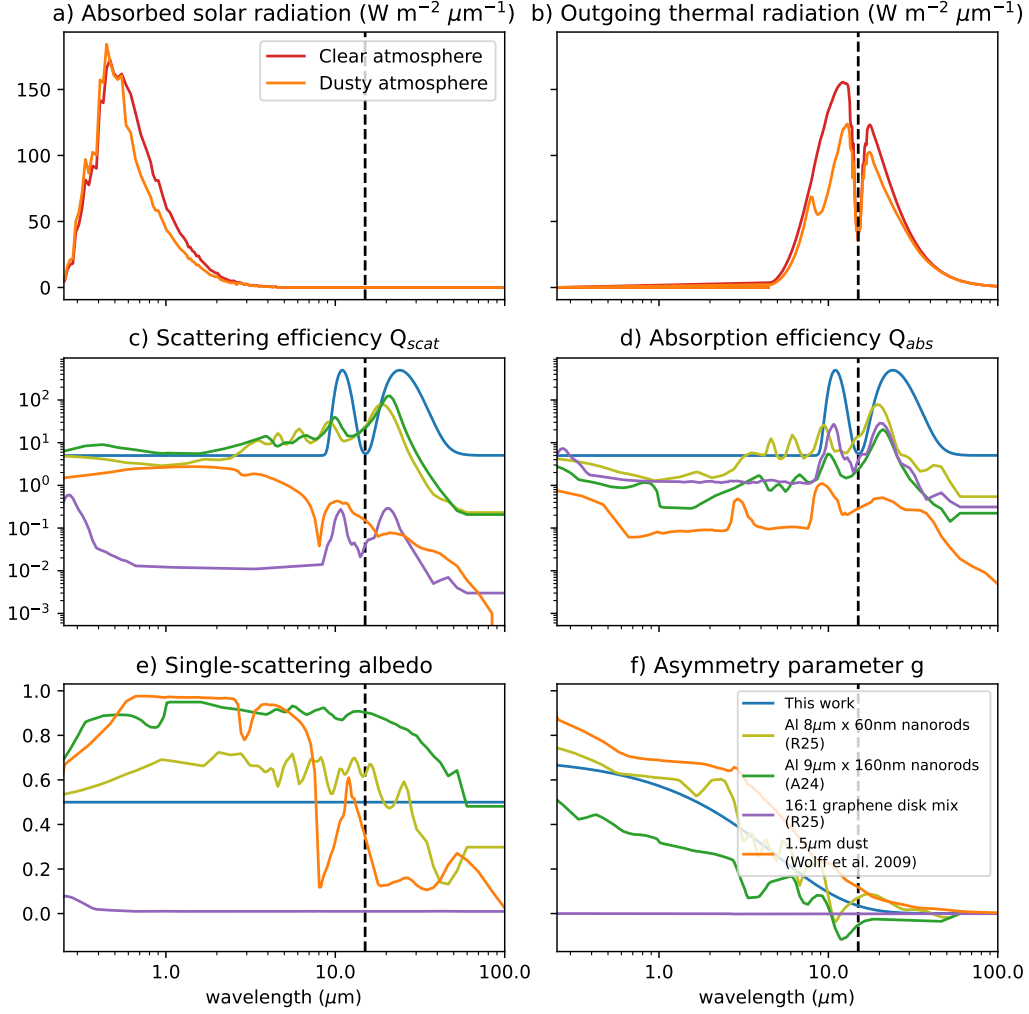


Figure 1. Top row: a) simulated insolation reaching the surface and b) simulated emission at the top of the atmosphere (multiplied by a factor of 20) for both clear and dusty conditions with optical depth $\tau = 3$, excluding the effect of engineered aerosols. The vertical black dashed line represents the $15 \mu\text{m}$ absorption band, where CO_2 absorbs efficiently (Kutepov et al., 2025). An engineered aerosol absorbing at $15 \mu\text{m}$ will have relatively little additional warming effect. c)-f): idealised Mars-warming aerosol optical properties, chosen to forward-scatter solar radiation to the surface while blocking surface thermal emission. We also show the spectrum of Martian dust with an effective radius of $1.5 \mu\text{m}$ (Wolff et al., 2009; Haberle et al., 2019) for comparison. Natural Mars dust lowers Mars dayside temperatures (Streeter et al., 2020), and is therefore not a suitable warming agent.

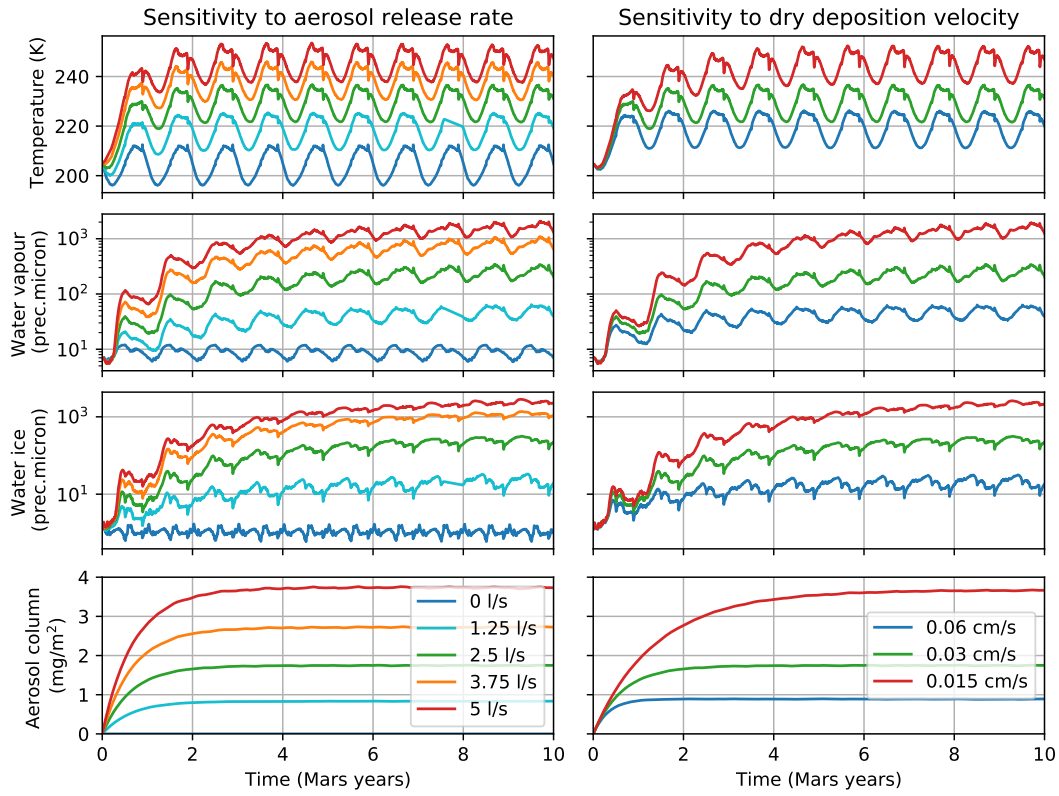


Figure 2. Evolution over time of, from top to bottom: global average surface temperature, atmospheric water vapour column depth, atmospheric water ice column depth and aerosol column depth. Results are shown as a function of (*left*) engineered aerosol release rate for a fixed dry deposition velocity of 0.03 cm/s, and (*right*) dry deposition velocity for a fixed aerosol release rate of 2.5 l/s. The model runs shown in this figure all correspond to scenarios with radiatively active water vapour but non-radiatively active clouds

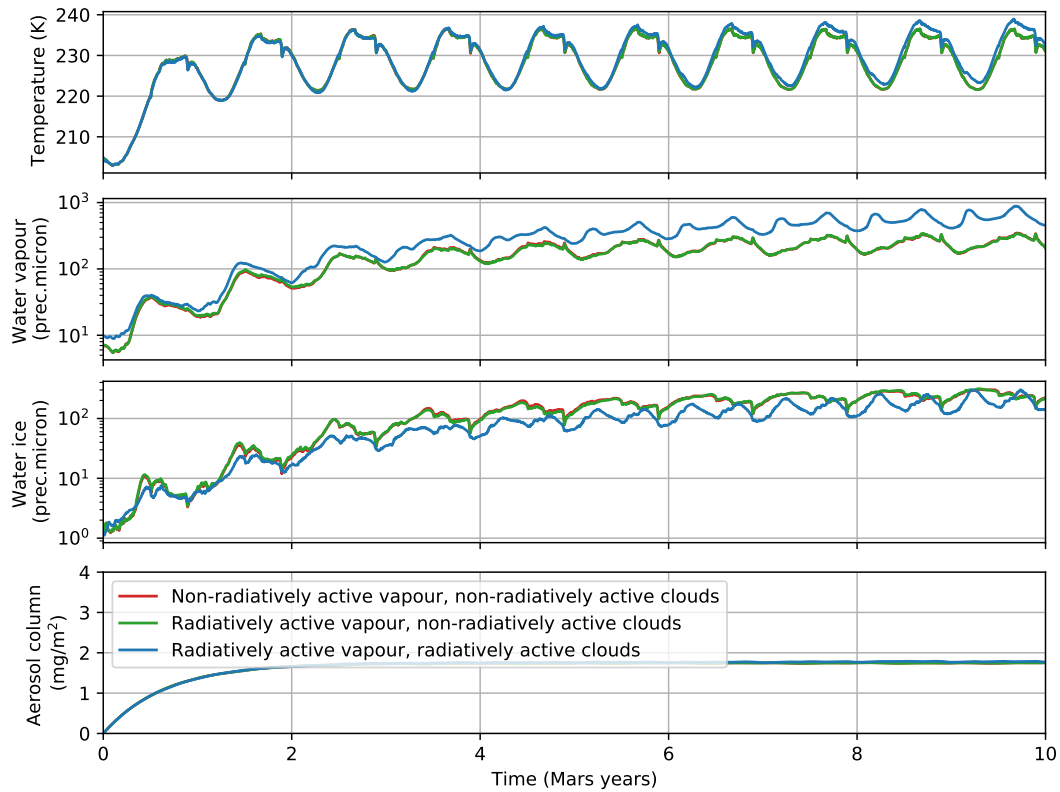


Figure 3. Evolution of global average surface temperature, atmospheric water vapour and ice column, and aerosol column depth for a 2.5 l/s aerosol release rate scenario. Results are shown for three different radiatively active scenarios. The two scenarios with non-radiatively active clouds are mostly indistinguishable from each other as the greenhouse effect from water vapour is weak.

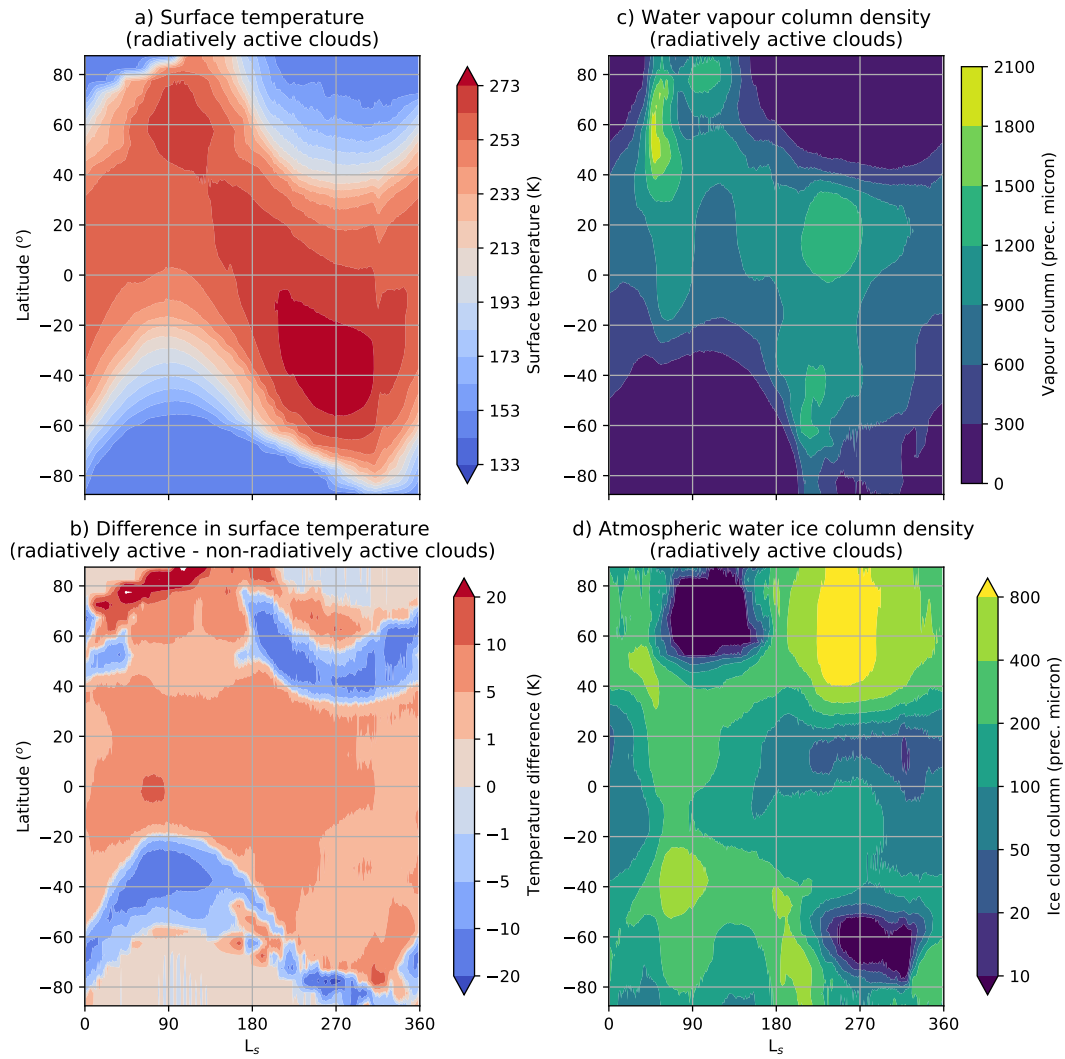


Figure 4. Seasonal variations in (a) surface temperature and (b,d) the atmospheric water cycle following 10 Mars years of aerosol release. (c) compares diurnally averaged temperature increase due to the direct versus indirect effect of radiative cloud feedbacks in the model.

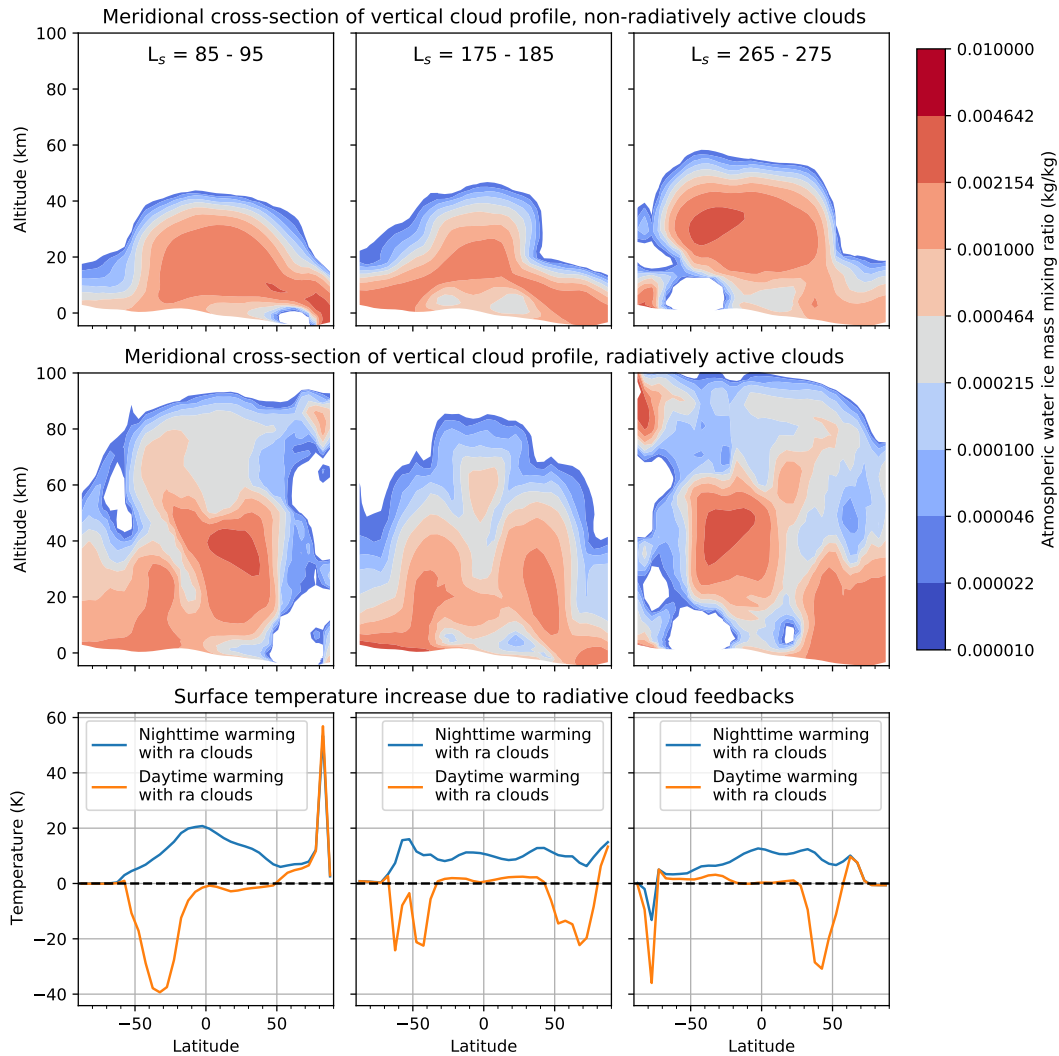


Figure 5. Zonal average meridional cross-sections 10 Mars years after start of aerosol release. Radiatively active ("ra") clouds warm the middle atmosphere, allowing for water vapour to rise higher in the atmosphere before condensing. Cloud belts over low- and midlatitudes therefore warm Mars during the night, while low-altitude clouds over the winter midlatitudes cause dramatic daytime cooling. Recession of north polar CO_2 ice cap results in strong water ice sublimation in Northern summer, and hence strong warming due to radiative cloud feedbacks.

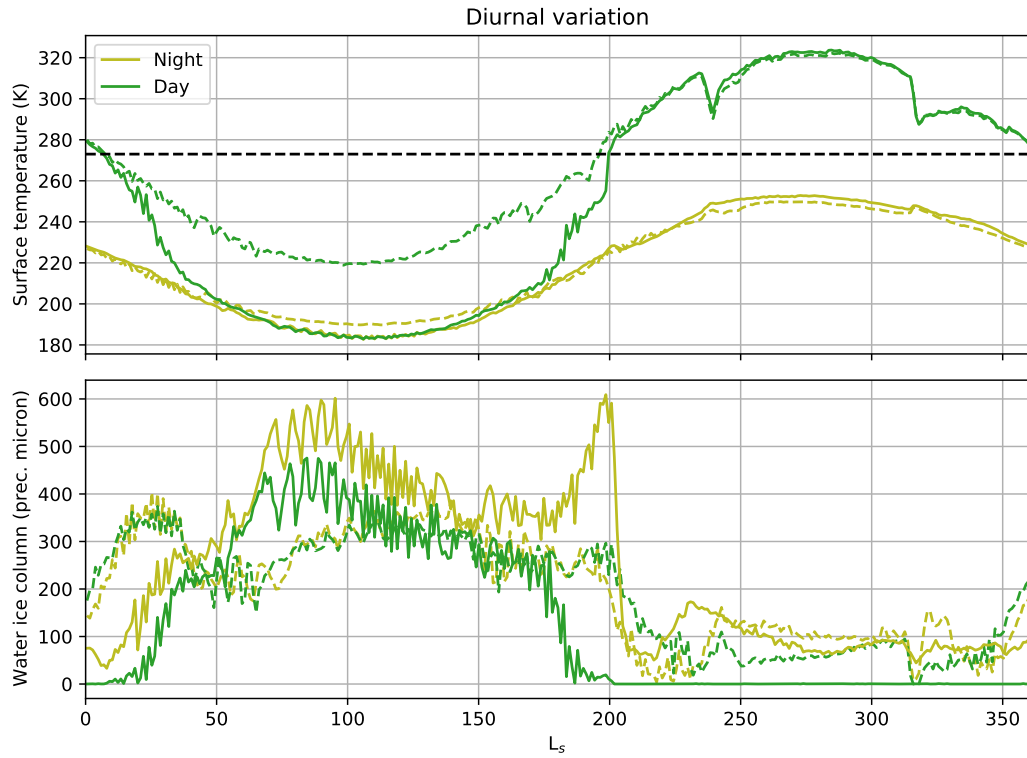


Figure 6. Radiative cloud feedbacks (solid lines) over the Hellas Basin (42° S, 70° E) cause dramatic daytime cooling in winter relative to when they are excluded from the model (dashed lines). In summer, the Hellas Basin warms by a few K during both day and night due to radiative cloud feedbacks. The figure above corresponds to the climate 5 Mars years after aerosol release starts.

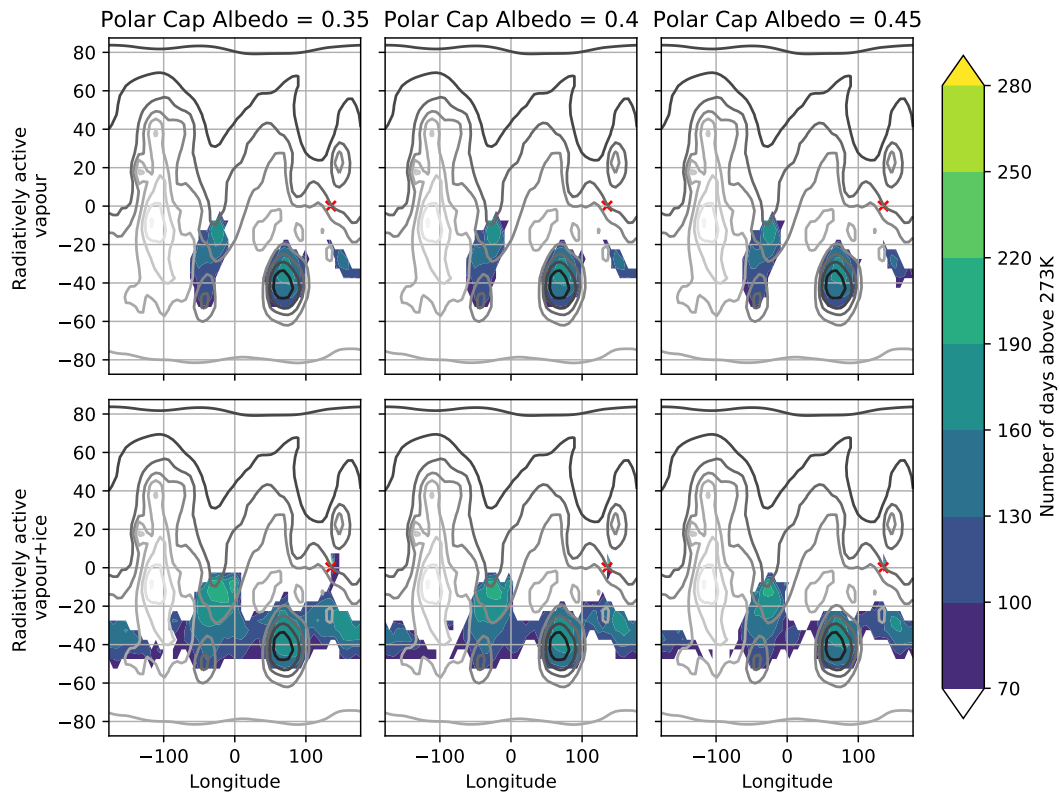


Figure 7. As the North Polar Cap albedo decreases, more of the Southern midlatitudes experience diurnal average surface temperatures above 273 K for more of the year, thanks to the effect of enhanced radiative cloud feedbacks (bottom row). If the effect of radiative cloud feedbacks are excluded (top row), warming sensitivity to albedo becomes negligible. The red cross indicates the aerosol release site. Grey contour lines represent surface elevation in 2 km increments.

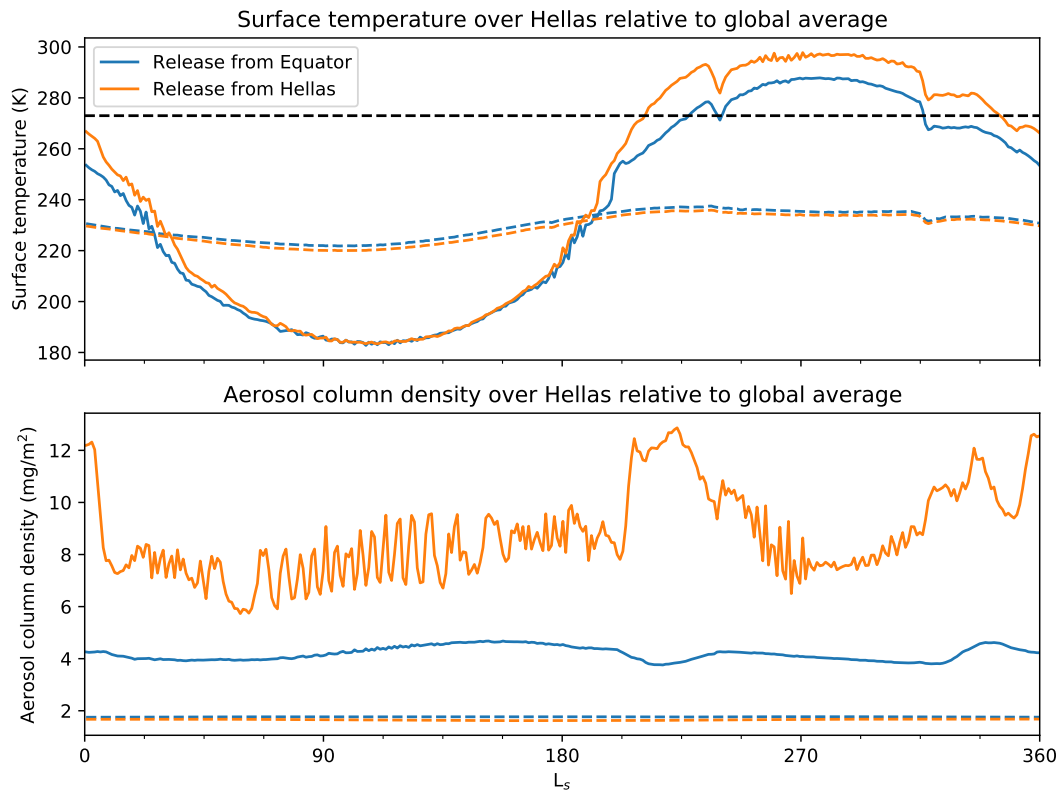


Figure 8. Within the Hellas Basin (solid lines, 42° S, 70° E), warmer summers can occur with an aerosol release site within the Hellas Basin instead of a release site at the equator due to the increased localised concentration of aerosols (solid lines, bottom), even if the magnitude of the aerosol release is kept the same. This causes a 10% reduction in global average aerosol column density in the atmosphere (dashed lines, bottom) and a small decrease in global average temperatures (dashed lines, top).

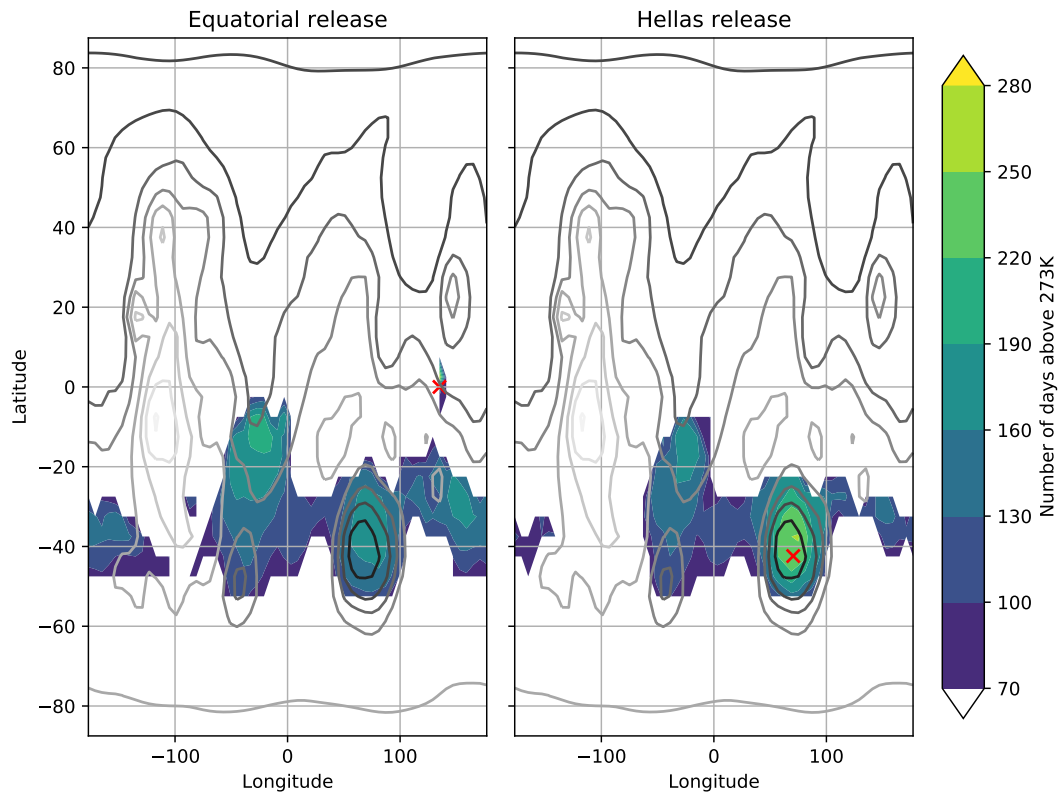


Figure 9. Changing the aerosol release site (red crosses) from Gale Crater (0° N, 135° E) to the centre of the Hellas Basin (42.4° S, 70.5° E) lengthens the warm season with average temperatures above 273 K within the Hellas Basin, while shortening the warm season elsewhere. Grey contour lines represent surface elevation in 2 km increments.

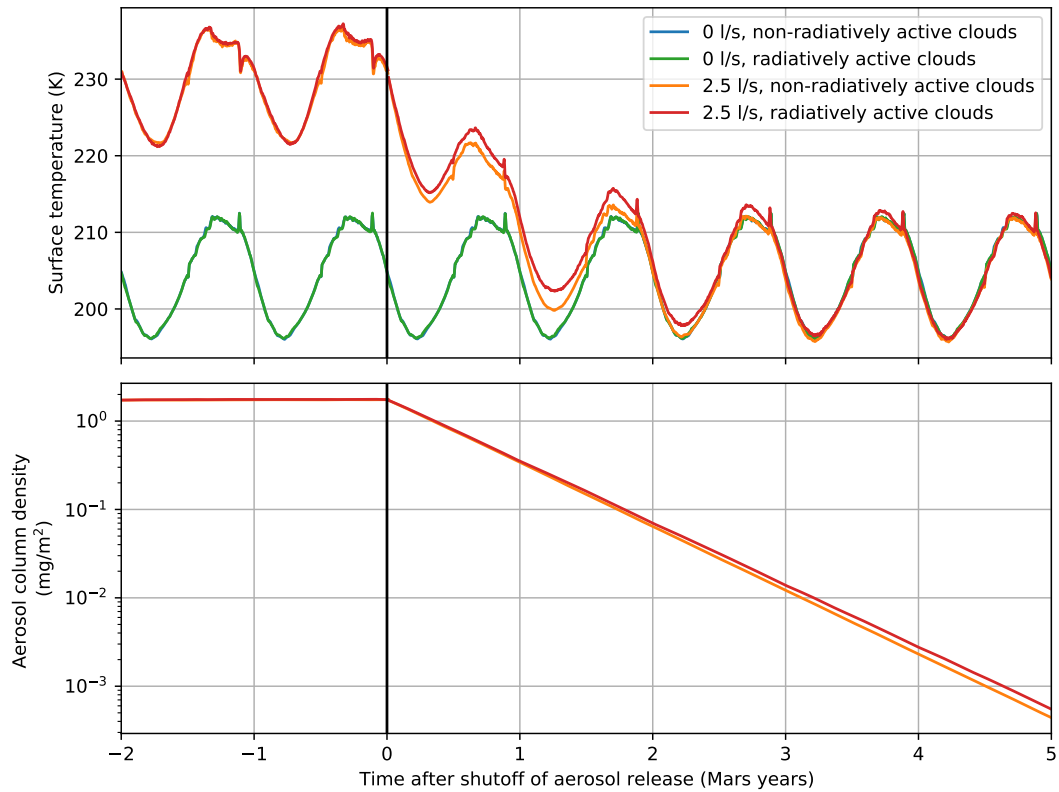


Figure 10. Upon ceasing aerosol release 5 Mars years after start of 2.5 l/s aerosol release, global average surface temperatures return to their pre-terraformed values (green line) within just a few Mars years as the aerosols are removed from the atmosphere on a 0.6 Mars year e-folding timescale. Radiative cloud feedbacks have little effect on aerosol removal timescales but slow down the reversal of aerosol warming.

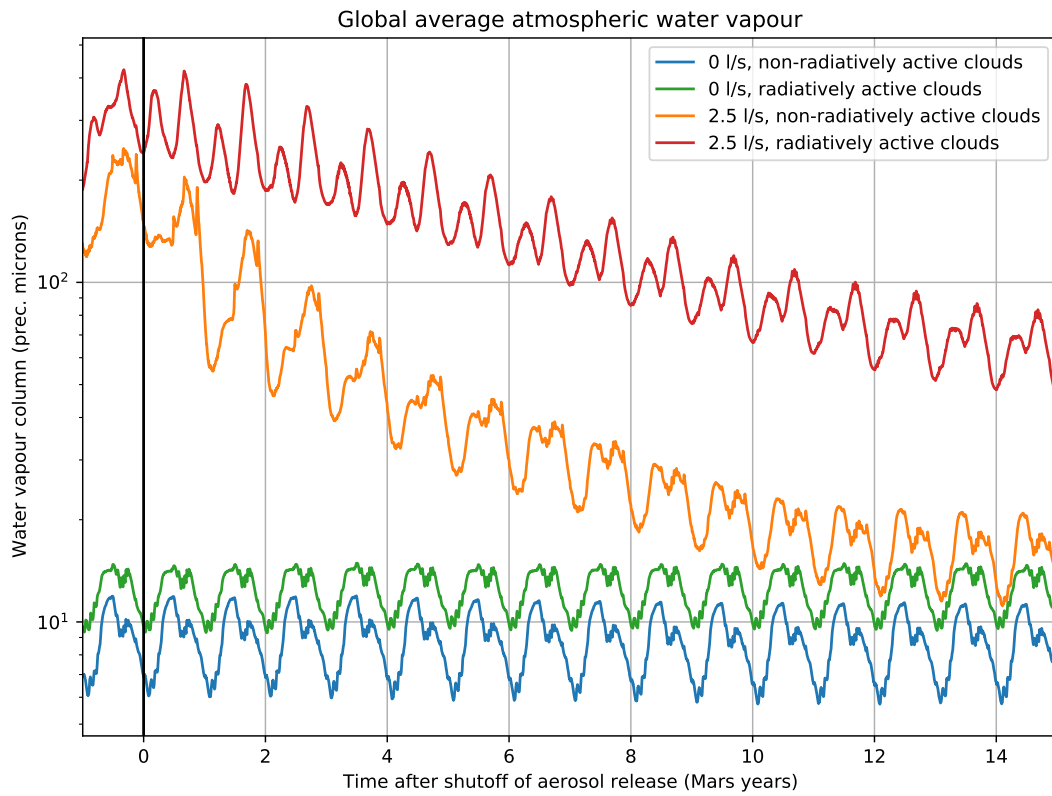


Figure 11. Global average water vapour content in the atmosphere only gradually declines following aerosol shutoff, eventually reaching a new equilibrium level dictated by the formation of the new South Polar cap. The decline is even slower if radiative cloud feedbacks are included as more water is stored seasonally in southern midlatitude frost.

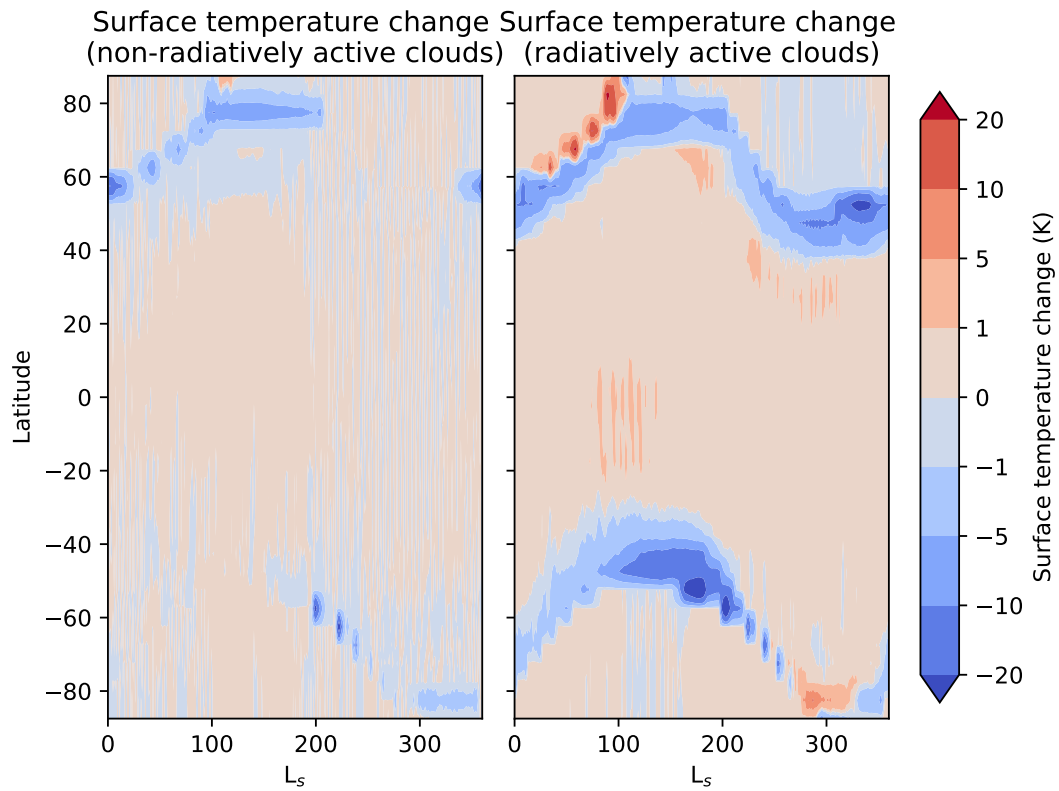


Figure 12. Surface temperature increase 15 Mars years after aerosol shutoff relative to the initial control case. Cloud-induced cooling in the winter midlatitudes persists for decades after aerosol shutoff.

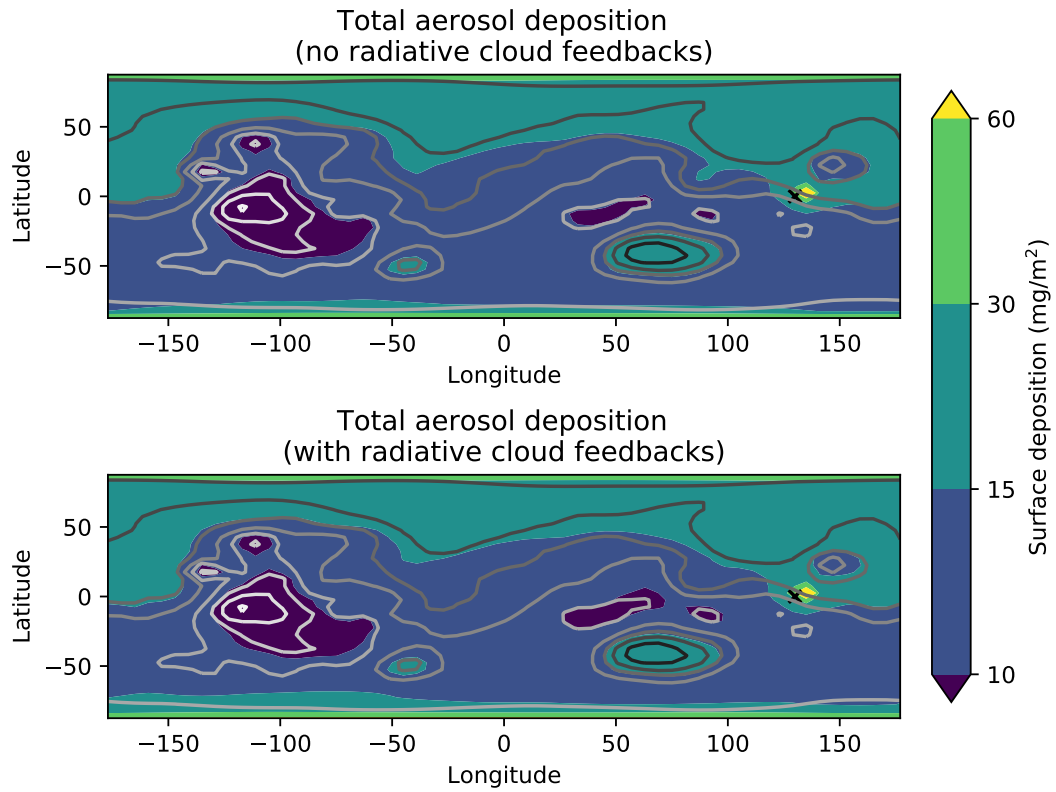


Figure 13. Aerosol deposition on the surface following 5 Mars years of 2.5 l/s release and 15 Mars years of shutoff. The distribution is comparatively uniform, with more deposition at low elevations, high latitudes and close to the release site (marked by the black cross). Including radiative cloud feedbacks makes little difference to the deposition.

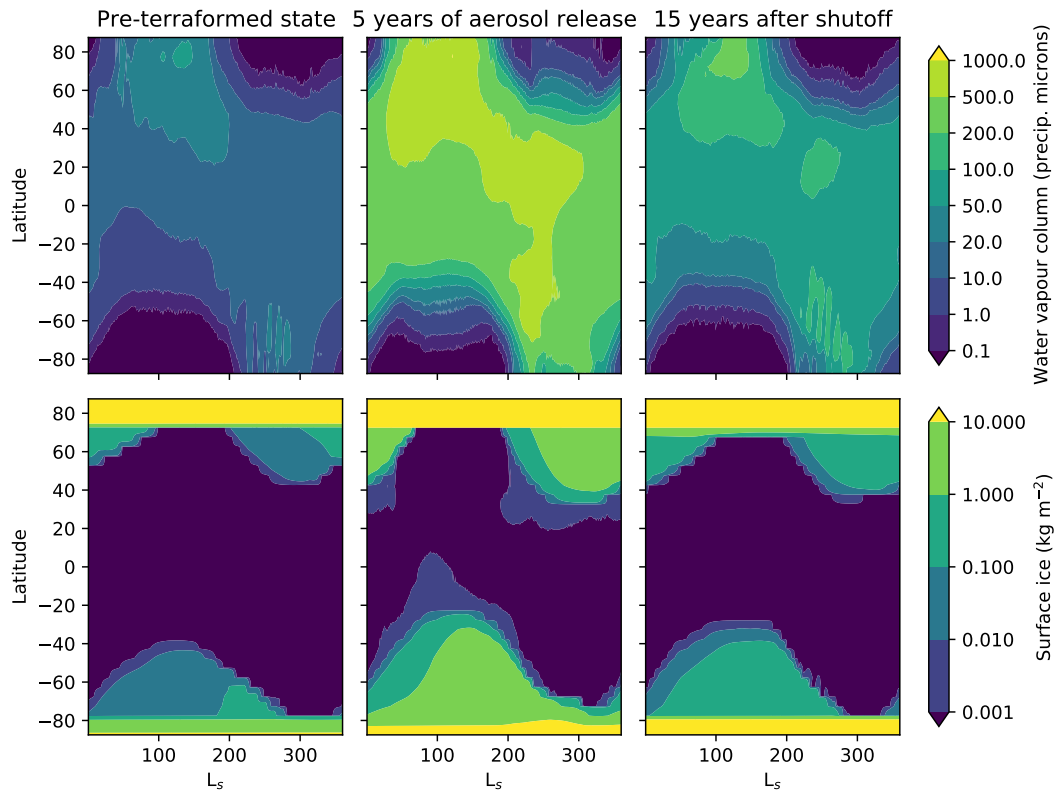


Figure 14. Warming of the Martian atmosphere (centre) results in an increase in atmospheric water vapour (top row) and thicker and more latitudinally-extensive frost in the winter midlatitudes (bottom row). Even 15 Mars years after aerosol shutoff (right), the atmosphere remains moist relative to its pre-terraformed state, winter frost remains thicker, and a perennial South Polar water ice cap remains.

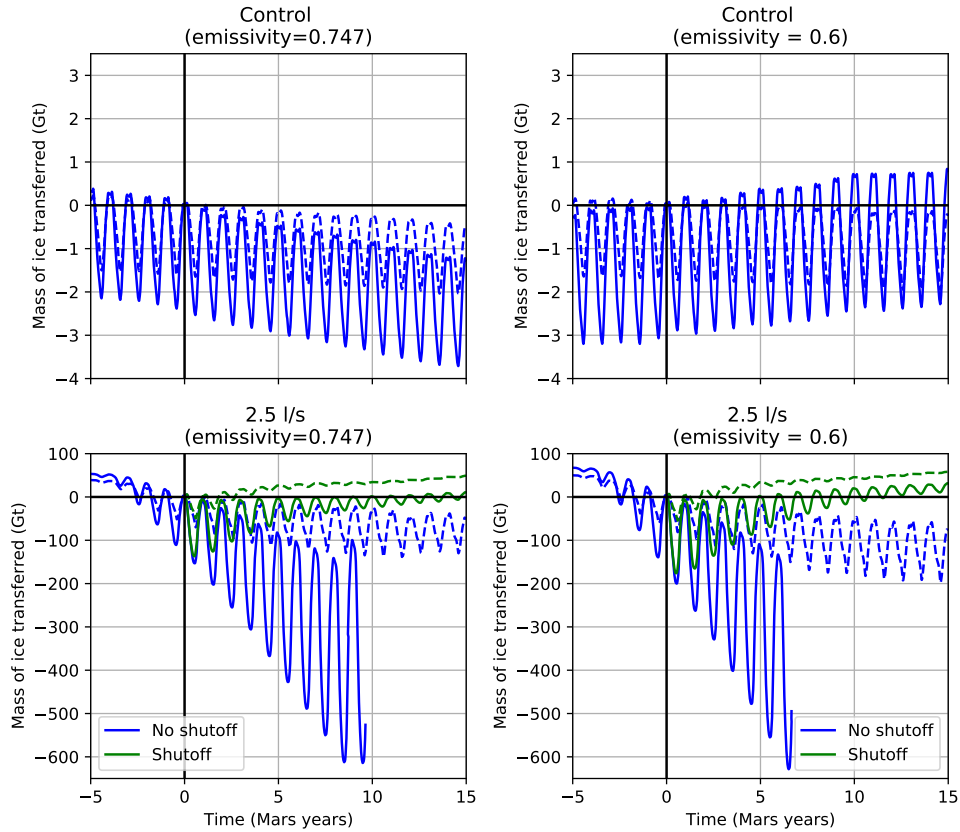


Figure 15. Difference between the northern hemisphere and southern hemisphere water inventory in the radiative (solid lines) and non-radiative (dashed lines) cloud feedback scenarios, normalised to the difference when $t=0$ (5 Mars years after start of aerosol release). Negative values indicate a net transfer of water from the Northern to the Southern hemisphere. Our model shows a small net bias in the control case of <0.1 Gt/year of water transferred from the Northern to the Southern Hemisphere (due to permanent deposition over the South Polar Cap) that can be eliminated or even reversed by reducing the emissivity of South Polar CO_2 ice. However, we model a consistent net transfer of water to the Southern Hemisphere during artificial warming regardless of CO_2 emissivity, that then reverses following shutoff. Our results are therefore robust to these model parameters.

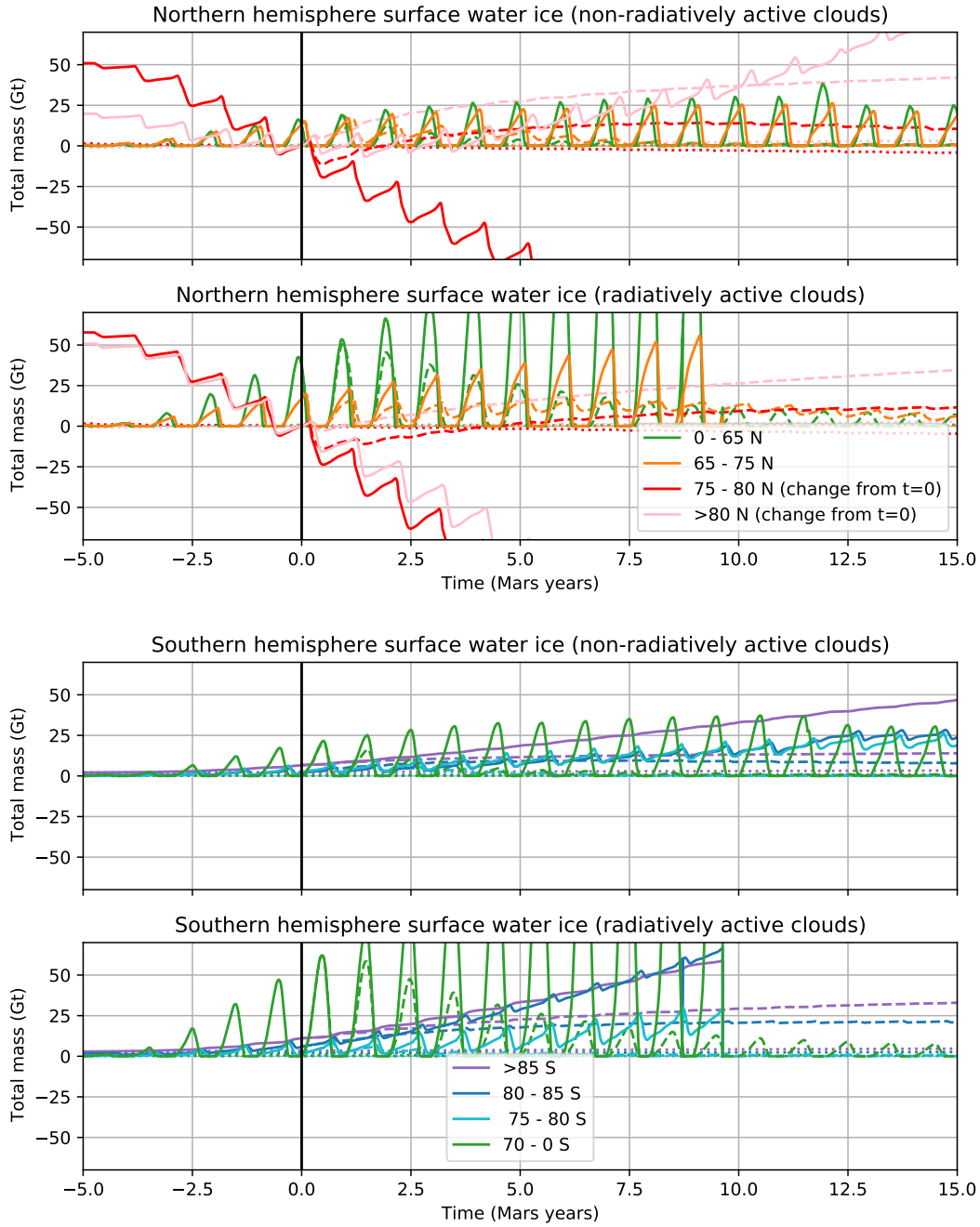


Figure 16. During aerosol loading, the South Polar Cap and midlatitude frost increases at the expense of ice sublimated from the edge of the North Polar Cap, and continues doing so if shutoff (marked as $t=0$) does not occur (solid lines). If shutoff occurs (dashed lines), water sublimates from midlatitude frost and is redistributed towards both the North Polar Cap and South Polar Cap. When radiative cloud feedbacks are neglected, the thickness of the edge of the South Polar Cap peaks after 9 Mars years before slowly declining. Radiative cloud feedbacks increase South Polar ice accumulation, with no decline observed within 15 Mars years after shutoff. Control values are shown in the dotted lines for comparison. Simulations with continuous aerosol release and radiatively active clouds become unstable after 15 Mars years and are therefore not shown after $t=9.5$ Mars years.

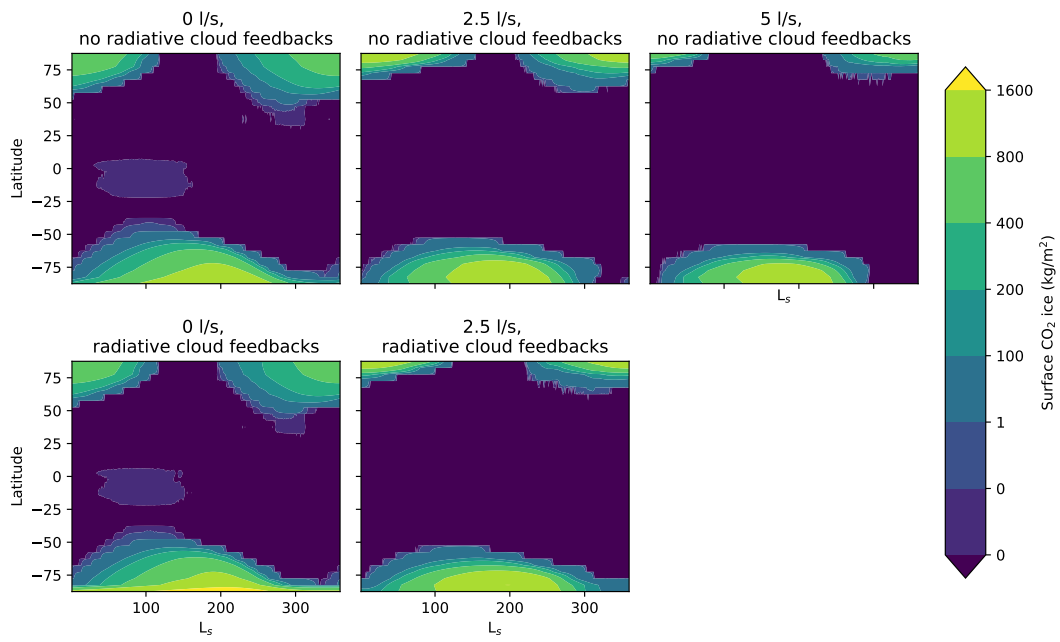


Figure 17. Seasonal CO₂ ice condensation continues to occur over the poles, with artificial warming causing a retreat in the latitudinal extent of the CO₂ ice cap but an increase in the thickness and seasonal persistence of the CO₂ cap.

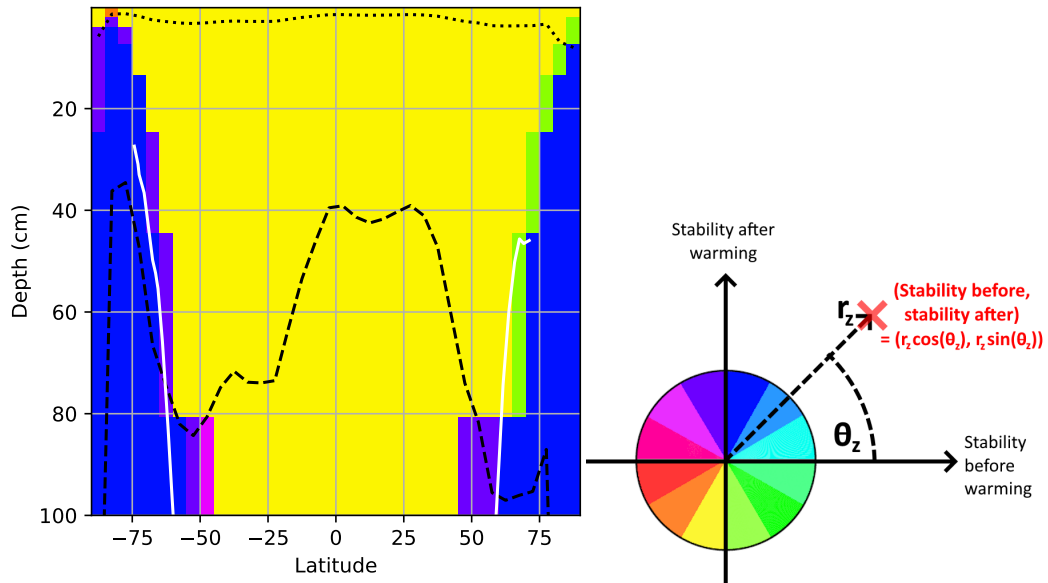


Figure 18. Zonally-averaged interannual stability of shallow subsurface water ice as a function of depth, comparing 10 Mars years of aerosol release with the control scenario. The dotted and dashed black lines respectively show the diurnal and seasonal penetration of thermal forcing, while the white lines show the predicted midlatitude ice deposit extent assuming no soil pore filling (Schörghofer & Aharonson, 2005). Colours correspond to the value of θ_z (legend on right). Ice is destabilised (green) from the Northern midlatitude deposit, and ice accumulates (purple and pink) in the Southern midlatitude deposit and at depths in the Northern midlatitude deposit less affected by seasonal forcing. Pore ice filling was neglected in this model; in reality the ice table in the mid-latitudes is likely to be shallower than our model predicts.

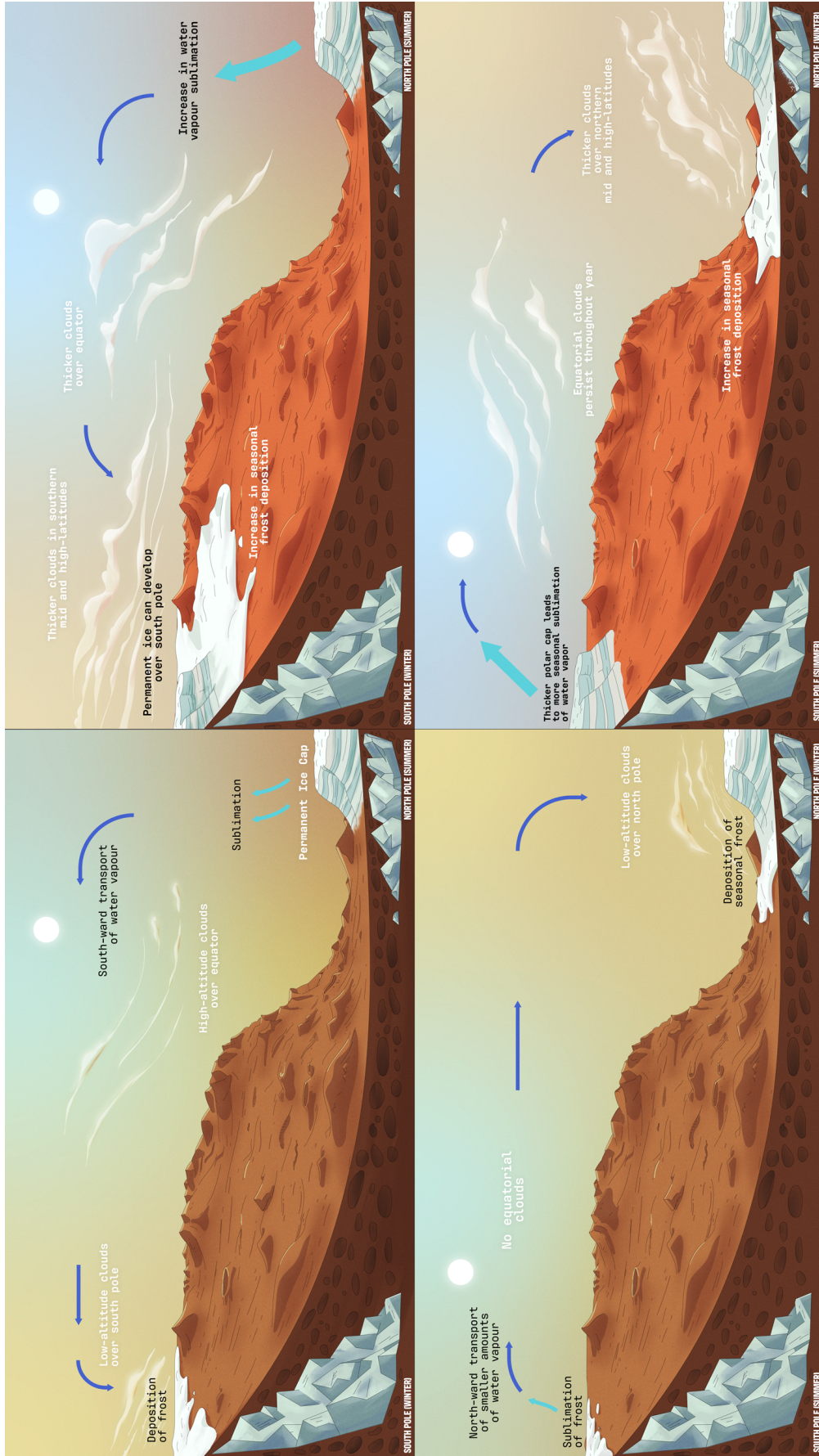


Figure 19. We summarise differences in the Martian water cycle between the existing modern Mars case (left) and the artificially warmed case (right), notably a) the increase in cloud cover and b) the increased participation of the South Pole in the water cycle. *Figure by Vlad Socianu*